

المدرسة التونسية للتقنيات

Institut Français du Pétrole



Tunisia Polytechnic School



French Petroleum Institute

Graduation project report:

2D finite difference modeling applied to Vertical Seismic Profiles

Achieved by: Moez AMRI

المدرسة التونسية للتقنيات (Tunisia Polytechnic School),

*Under the Supervision of: Charles NAVILLE,
Institut Français du Pétrole (French Petroleum Institute)*

Academic year 2005/2006

AIGION FAULT CASE*:
MODELING PROCEDURE AND
RELEVANT RESULTS

*This chapter is the subject of a scientific paper.

Introduction:

In the present chapter we intend to refine the Aigion fault structural model obtained from previous scientific works (*Place and al. 2005*). The Aigion fault context is not geologically complicated however the conventional seismic reflection technique gives very poor results and does not image any reflector. Thus, using the 2D full wave modeling technique, this work will be based on the reconstitution of the seismic wave propagation through the geological structure of the AIGION fault vicinity in order to confirm the relevant structural information. In the Aigion fault case, only refracted and diffracted waves could be analysed and used to identify major structural features in the fault vicinity. These arrivals are rarely used in industrial well seismic to derive any structural information.

The 2D modeling of the fault will be based on the previous analysis of the VSP data recorded in the well AIG-10 and the relevant results of the well logs and geological observations. (*EU project «3F-Corinth»*).

2.1. Summary of the Aigion fault structural knowledge.

2.1.1. Presentation of the case study:

The case study is located in Greece, on the south border of the Corinth Gulf. The Aigion fault is an E-W oriented structure outcropping in the western part of the gulf and dipping at 60°N (*Micarelli et al., 2003*). The Aigion fault is an active fault bordering the gulf (Aigion city has been partially destroyed by a recent earthquake in 1995.)

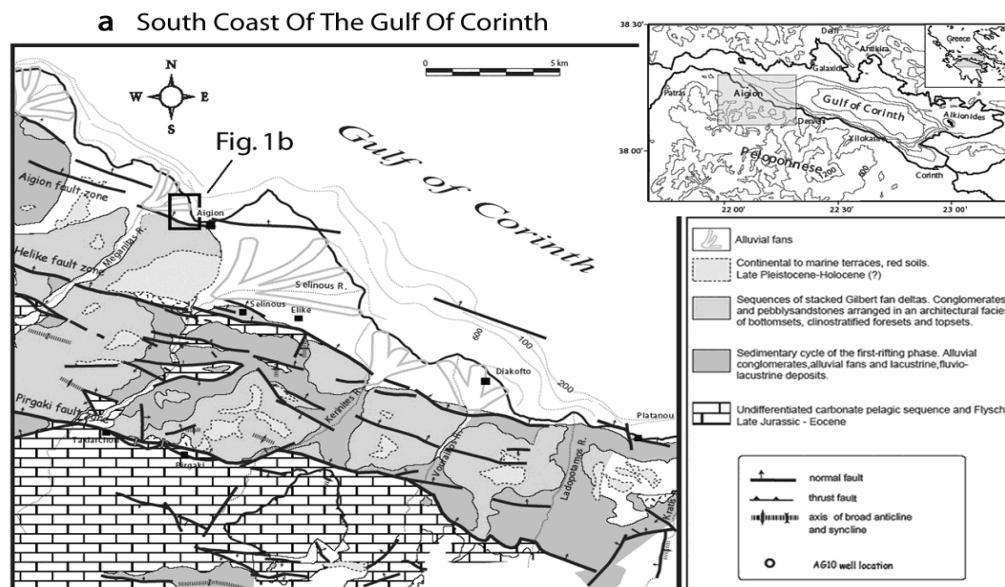


Figure 2. 1: Map of the south coast of the Gulf of Corinth (SE of Aigion), modified after *Micarelli et al. (2003)* and *Frima et al. (2004)*.

The Aigion fault keeps a constant angle of 60° over the shallow 1000 m depth interval, as the other outcropping faults of the area (Helike and Pirgaki F). Indeed the fault has been intersected by the scientific well Aig-10 at 760 m in depth and successfully cored. Its 60° dip is confirmed by the AIG-10 well (Cornet et al., 2004).

The objective of the Aig-10 well was to core and monitor the Aigion fault: the rig has been positioned at 415m from the fault.

2.1.2. Geological column at AIG-10 well:

The characterisation of the geological formations in the well vicinity starts with the examination of the relevant borehole data: coring and core description, well logging (sonic and gamma ray logging) .The exploitation of these data leads to the following geological structure assessment:

Superficial layer (0 to 127 m)

The superficial low velocity layer is very heterogeneous; it consists on an intercalation of sandy gravels with clayey and slimy layers. It consists mainly on fluvial deposits coming from Meganitas river.

Consolidated conglomerate (127 to 388 m);

At this depth level, the well had encountered stiff conglomerates with clastic limestone, marl, and radiolarite.

Clay (388 to 500 m)

At this level we encounter clayey-sandy alternation with fluvial deposits.

Radiolarite and platy limestone (500 to 700 m)

At this deep range, appears dense layer of platy limestone, marl, and radiolarite. Heterogeneities affect this lithological sequence which assess for the presence of some secondary tectonic contact and the crystallised calcite recovered from this zone are due to fluid circulation.

Olonos Pindos limestone (700 to 760 m)

These limestone have platy structure like the upper layer but they are less altered by alternation.

The fault:

The well crosses the fault at 760 m. The dip of the fault measured using the borehole data (~ 60°) is coherent with large scale dip measurement .The fault contains a 50 cm thickness radiolarite layer.

Limestone of Tripolitza (770 to 1000 m)

From 770 m down, the well encounters limestone again. The high water pressure existing in this zone (5 to 10 bars) prevented the recovery of drilling cuttings. But later data and sample collection of water shows that it is the Tripolitza aquifer. Deeper, the limestone becomes porous and highly fractured and the dissolution structure suggests the development of a karstic zone.

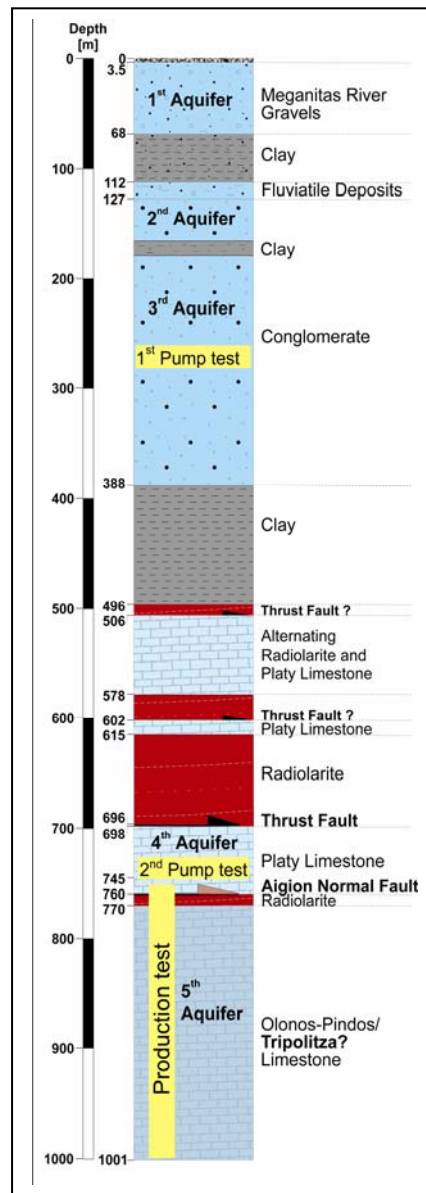


Figure 2. 2: Identified Lithology in the AIG-10 well.

2.1.3. Standard VSP data processing and interpretation:

2.1.3.1. The VSP survey in the Aigion area:

Initially, the VSP survey was undertaken to calibrate the surface reflection images, and possibly refine the image of the Aigion fault vicinity. Unfortunately, as the surface seismic did not yield any reflection results, the mini 3D reflection survey, initially planned, had been cancelled. And the VSP was the only data left to tentatively assess the Aigion fault geometry and to determine its actual structure.

6 VSPs were recorded: one Zero Offset VSP (VSP#1) and five Offset VSPs scattered all around the well head (**Figure 2.3**). In the borehole, the VSP tool contained 3 orthogonal geophones \bar{x} , \bar{y} and \bar{z} , and a hydrophone. Although this association of sensors is efficient to interpret the different seismic arrivals, it is rarely used in the industry. Due to operational circumstances, no data were recorded on the footwall below 755m.

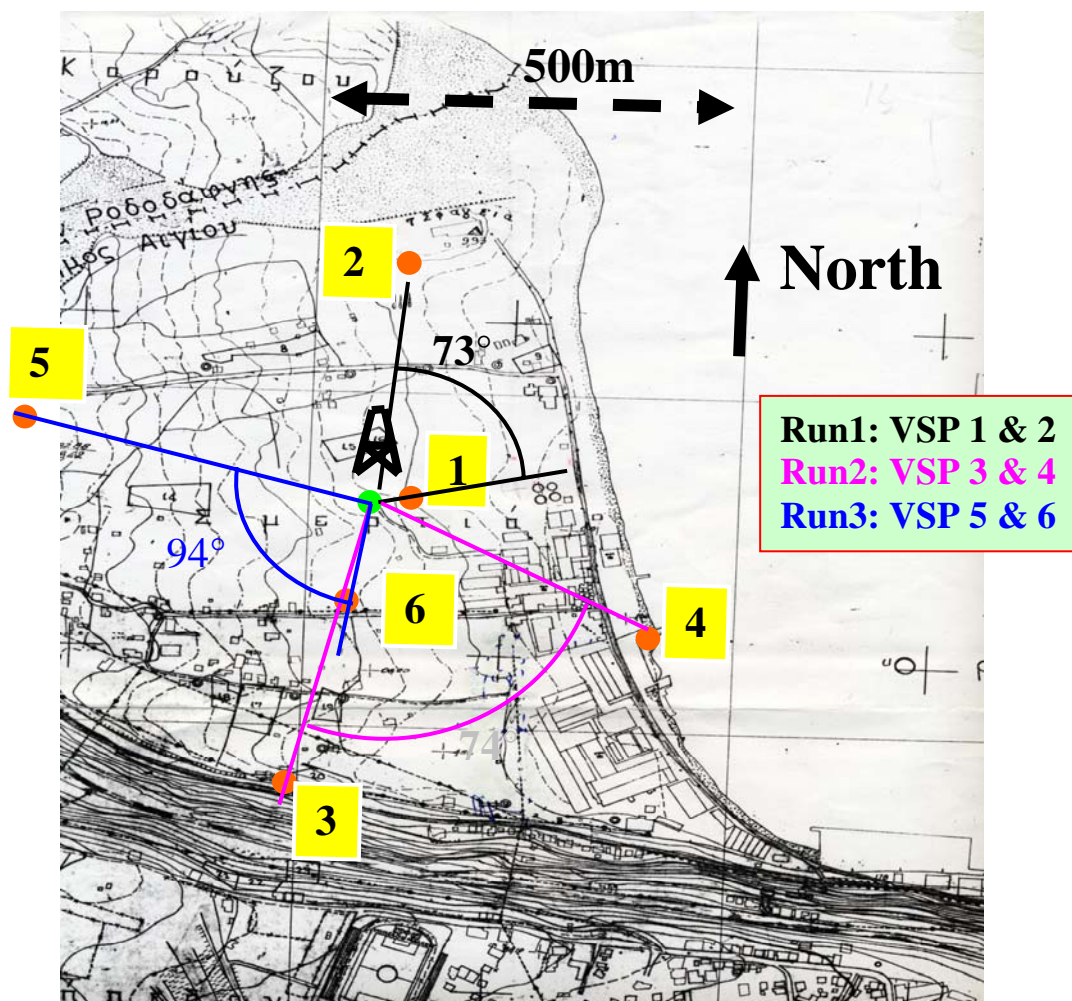


Figure 2. 3: The VSP position and the scarp of the Aigion fault. (1) is zero offset VSP, others are offset VSPs . Note the position of VSP#3 near the fault (EU project " 3F-Corinth").

Standard VSP processing results have been produced, such as time picks, velocity curves (in P and S-wave modes) presented in **Figure 2.4**, accompanied with the sonic log (P wave) .

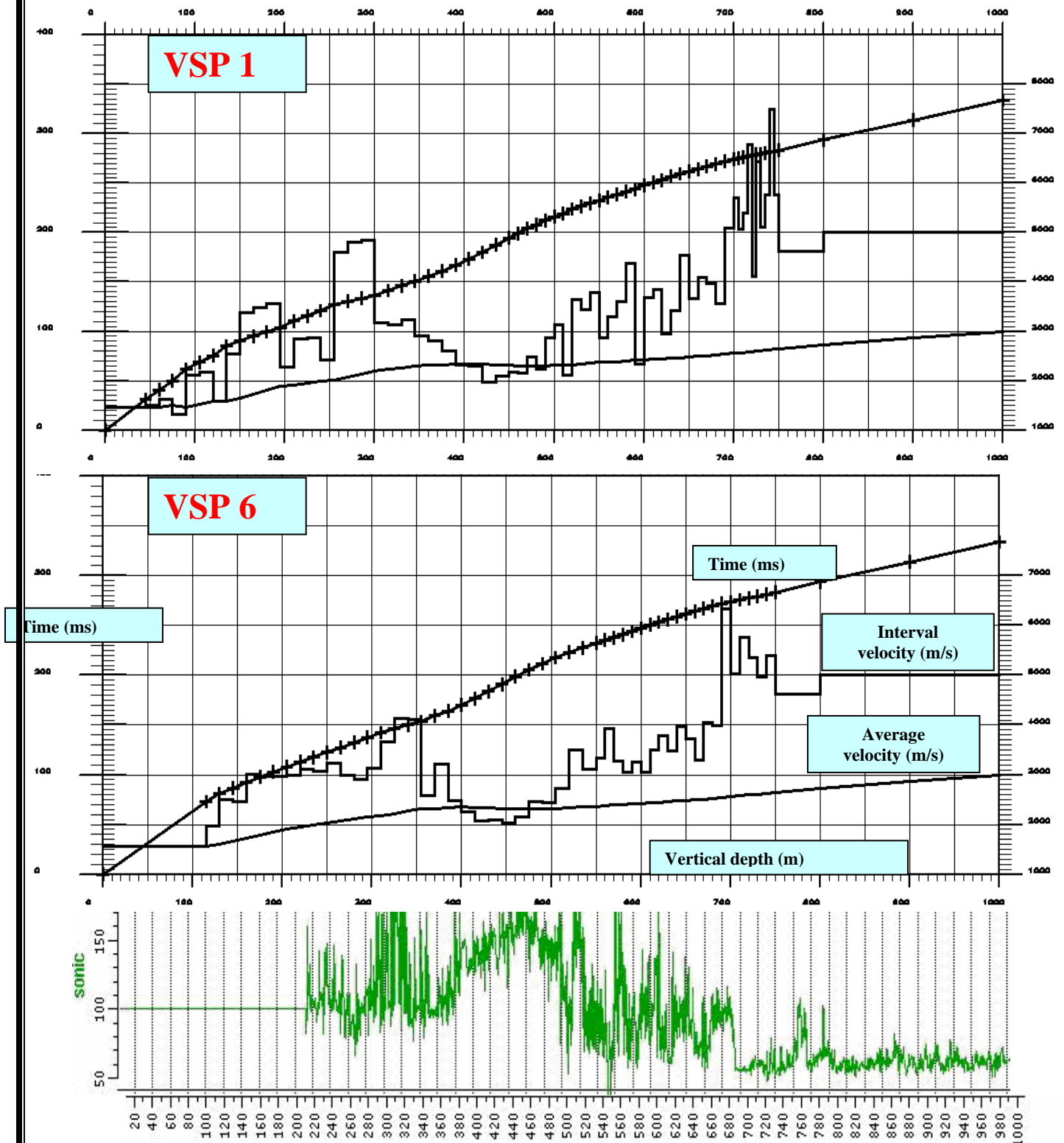


Figure 2. 4: Sonic logs and P-wave Time and velocity curves versus Depth (*EU project " 3F-Corinth"*).

Surprisingly, in spite of major velocity contrasts expressed by the sonic log and by the interval velocities derived from direct arrival VSP times, the 1C, 3C or hydrophone VSP processed results do not evidence any clear P-P reflected event, only few coherent P-S converted reflected line-ups appear after velocity filter removal of the downgoing P-wave train (*EU project " 3F-Corinth"*). Thus, high energy direct, diffracted and refracted arrivals have been studied in order to glean any structural information.

2.1.3.2. Recorded VSP seismograms analysis and interpretation:

The investigation of VSP data and direct wave incidence revealed that the fault signature on wave propagation is obvious in VSP3. **Figure2.5** shows two VSP records (VSP5 and VSP3). On VSP5 we recognise the direct P wave arrival, its high amplitude near the wellhead decreases while travelling downwards. Thus, no abnormal events are detected during the wave travel path and the fault does not manifest any effect on the VSP5 direct arrival. On the other hand, VSP3 exhibits complex arrivals:

- The direct arrival (1) at shallow levels is abnormally weaker than in depth, in contrast with all other 5 VSPs.
- A high energy signal (2) having a hyperbolic pattern appears around 520 m.
- A weak signal (3) appears in first arrival around 650 m as a linear line-up.

The effect of the Aigion fault is clearer in VSP3. Thus, VSP3 was mainly used to extract the structural information related to the observed diffracted and refracted events and to build primary model that summarises all the relevant observations.

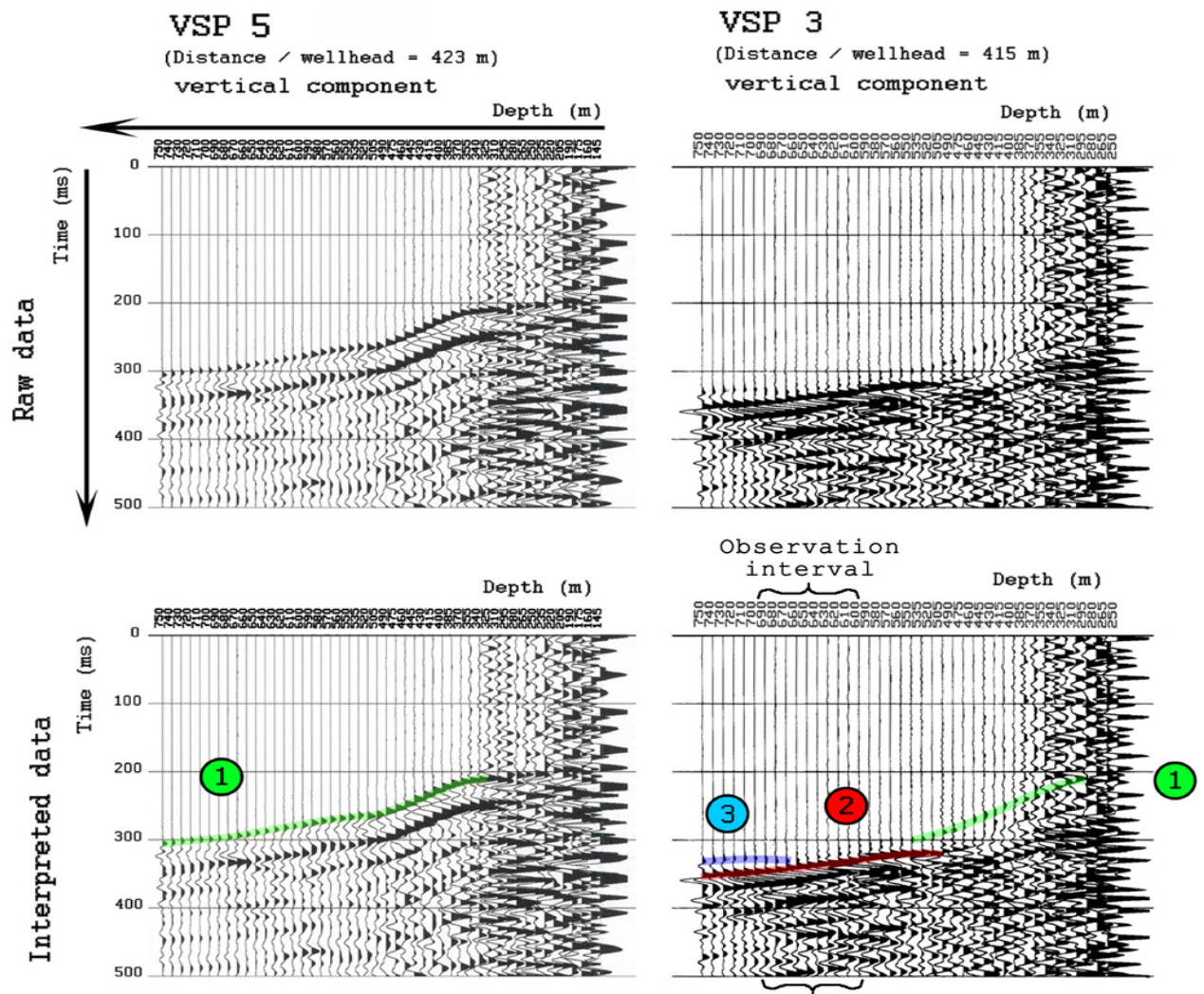


Figure 2. 5: Recorded VSP seismogram: left column: raw and interpreted VSP6 data, right column: raw and interpreted VSP3 data

Wave (1):

The signal 1 (**Figure2.5**) is the geophone response of the direct first arrival: i.e. propagation in the hanging wall compartment. This P-wave signal is more visible in the vertical component than it is in the horizontal one. On VSP 3, the weak amplitude of arrival (1) in the shallow depths reveals that it travels through a highly fractured and attenuating zone.

Wave (2):

The high amplitude signal (2) has a hyperbolic pattern with an apex situated at depth ~ 520 m \pm 20 m (**Figure2.5**). A diffraction phenomenon is likely to explain the hyperbolic profile and the incidence of this wave. In fact, while baffling the geological layers, the fault creates sharp corners favouring the generation of the diffraction events. This wave was detected by the hydrophone which confirms its P wave nature.

The observed diffraction apex is likely to be situated around 520 m, which corresponds to the top of the radiolarite and platy limestone layer. In fact the examination of the velocity curves (VSP1 and 6) shows an abrupt velocity contrast at this depth which might generate such a diffraction if intersected by a fault located laterally to the well.

Below 630m, the wave (2) incidence becomes, suddenly, horizontal and unstable. This transformation is certainly due to the interference with the wave (3) that starts to appear at this depth.

Wave (3):

Wave (3) (**Figure 2.5**) is observed in first arrival from 650m. This P-wave exhibits a near horizontal incidence regardless the depth, and it does not follow a clear hyperbolic pattern. The fact that it is observed in first arrival evidences that it propagates through the high velocity limestone formation (5000 m/s) located laterally to the well. This observation testifies refraction propagation along the fault plan.

2.1.4. Velocity Model of Aigion fault vicinity:

The investigation of the available data (geological observations, sonic logs, and VSP data) leads to the assessment of a velocity model (**Figure 2.6**) built by horizontal extrapolation of the velocities from well location to the hangingwall. In the footwall, all layers have been shifted upwards with the vertical fault throw of 200m, estimated by *Place et al. (2005)*¹.

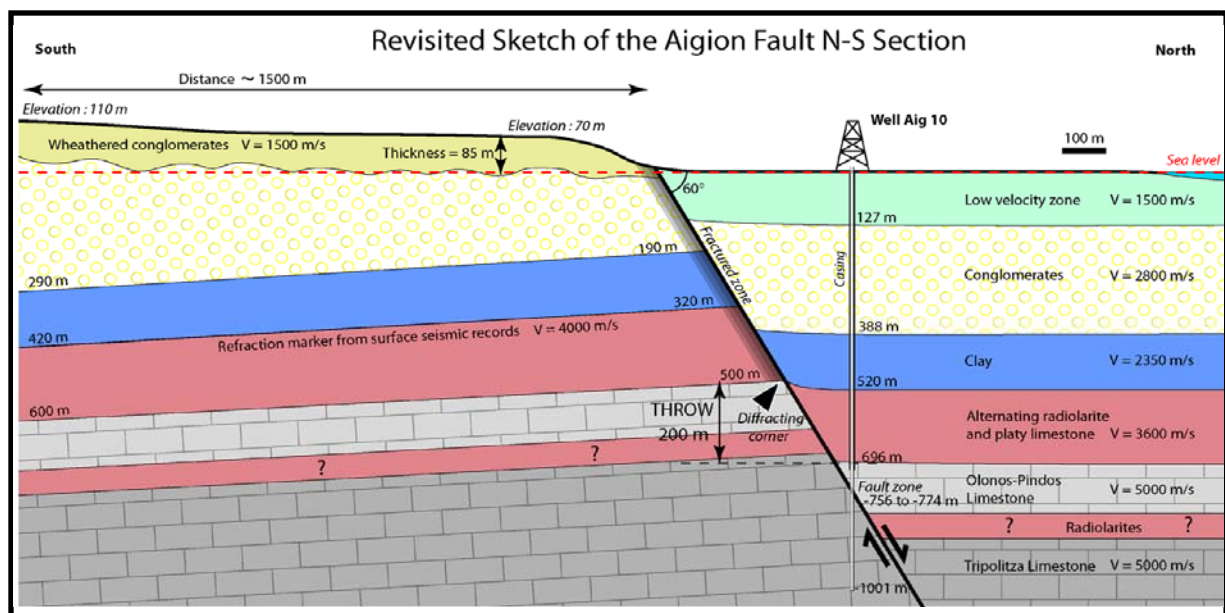


Figure 2. 6: Available velocity model of the Aigion fault vicinity (*Place and al. 2005.*).

¹ An arrival time based technique was developed to assess the fault throw.

2.2. Reconstitution of representative VSP seismograms in the Aigion fault vicinity using 2D finite difference modeling:

As stated in the above paragraphs, in spite of the excellent quality of the acquired data, it occurred that VSP reflection processing did not show any consistent reflection event, either from standard mono-component (1C) VSP processing, or from advanced three-component (3C) VSP processing (*EU project " 3F-Corinth"*). Consequently, in order to derive some structural information, the VSP processing have been focussed on the detailed analysis of the high amplitude diffracted and refracted seismic events observed on the 4C data, these events are generated by the presence of fault edges and fault planes in the AIG-10 well vicinity.

The synthetic 2D full wave modelling of the fault is a precious technique to help understanding the origin of the major seismic events recorded in the VSP data such as refraction and diffraction events which cannot be modelled properly by ray tracing.

The aim of this work is to confirm the model suggested by (*Place and al, 2005*) and derive additional structural information. In fact, based on the 2D full wave modelling technique, we will gradually modify this model up to regenerating the major seismic events observed in the real VSP data.

2.2.1. Modeling tool settings:

The 2D finite difference full wave modeling tool allows the simulation of the wave field propagation in a given geological structure. Building the model starts with designing the 2D density-velocity structure of a geological cross section. For each geological layer or zone the shear wave and compression wave velocities (V_s and V_p), and the densities values, are defined.

Once the model sketch is built, source and receivers parameters should be set. In fact, in the case of the Aigion fault modeling we used the following settings:

Source: 1 exploding point source with a 100Hz central frequency and generating a symmetric wavelet seismic field in all direction;

Receivers: geophones are distributed along the vertical well from 100m to 1000m depth 10m apart.

Calculations of grid settings including time and space grid cell size are automatically determined from two input parameters taken from the model data:

- a) Minimal compressional velocity (in the given model);

b) The peak source frequency.

The cell size is calculated from the stability and non dispersion criterion mentioned in the first chapter. In some cases we will define manually the grid size (smaller than the automatically defined size) to avoid shear wave dispersion (S wave usually has much smaller wavelength value) and computational noise and artefacts.

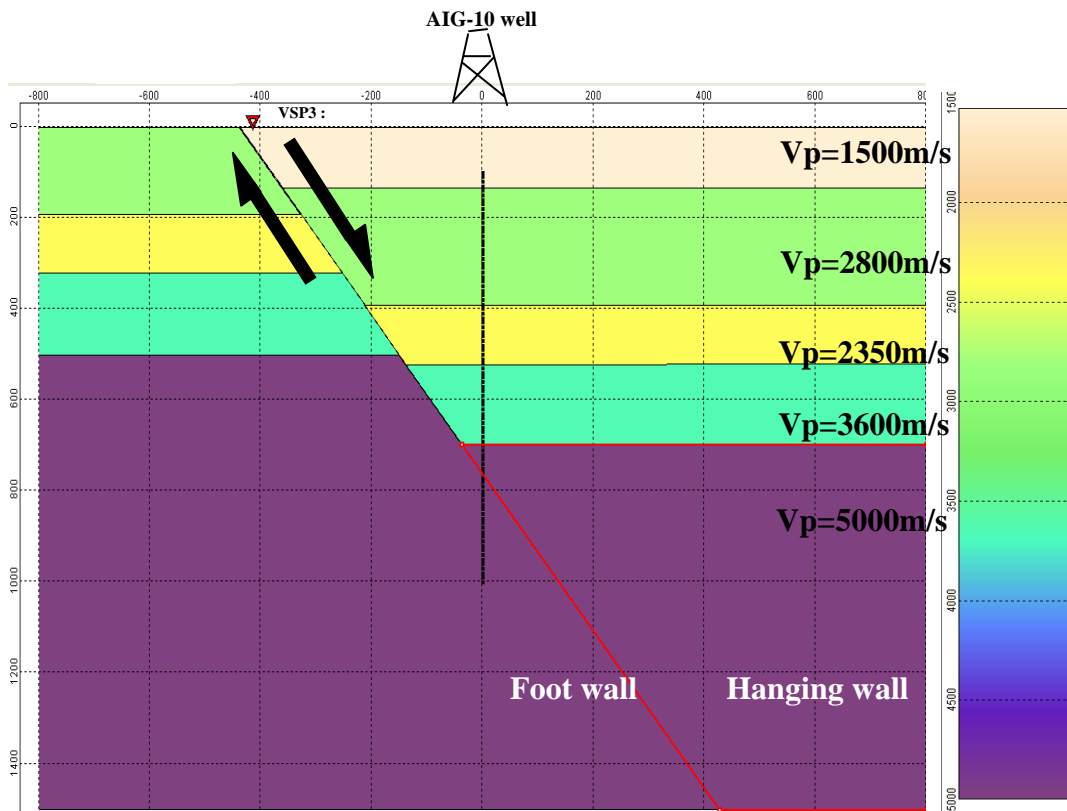
At each modelling step both elastic and acoustic simulations are run helping the differentiation of shear (S) and compression (P) arrivals. And, both horizontal and vertical components are investigated.

2.2.2. Modeling procedure:

In this paragraph we describe the modeling procedure steps that were achieved. In fact, through gradual modification and simplification, we intend to understand the wave behaviour in the created models and determine mainly their travel paths. This technique allows for generating the desired events recorded in the field data and defining the related geological structures.

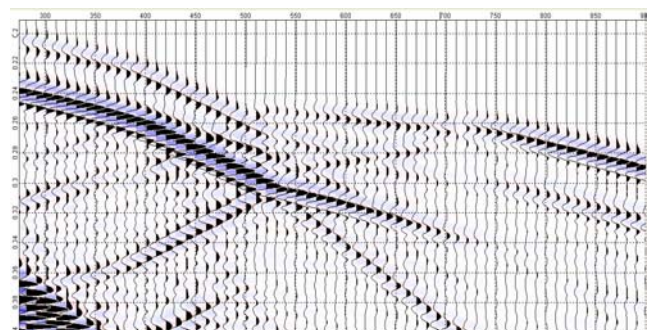
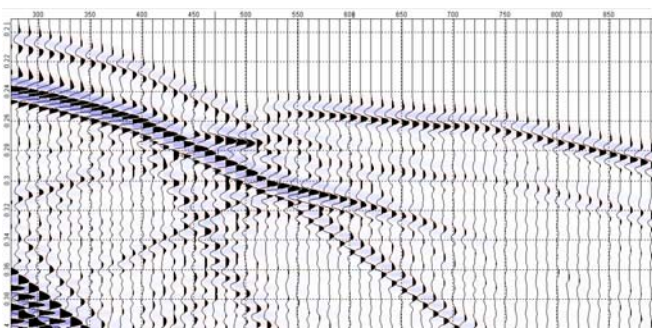
Model 1:

The first step in the modeling procedure is to build the velocity model of the fault vicinity as suggested in previous publications. In this cross section sketch, we simplified the surface conditions and assumed that it is a perfectly horizontal boundary. This assumption will not affect the generated results as the main events are observed on subsurface receivers.



Elastic vertical component

Elastic horizontal component



Acoustic vertical component

Acoustic horizontal component

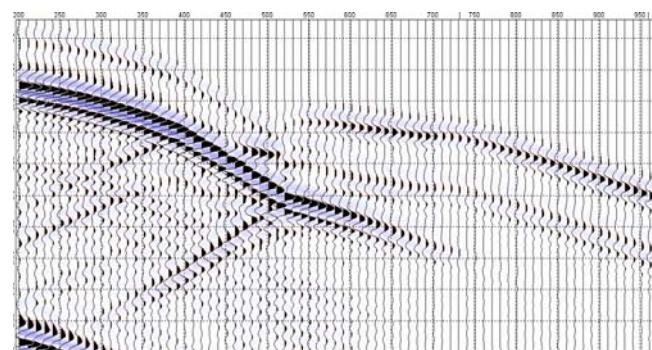
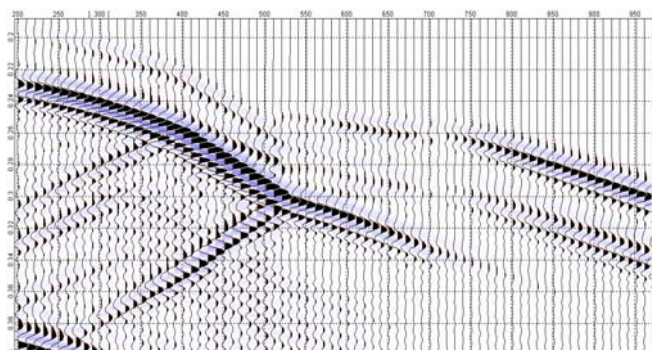


Figure 2. 7: Model 1 and the generated seismograms. note the double direct arrival and the complicated wave patterns generated in this model

The generated seismograms exhibit complex wave fields. In fact, we mainly observe a double direct arrival unseen in the real VSP data, typical of the presence of an accident near the seismic source location. This observation can be explained by the fact that seismic field energy travelled through the high velocity conglomerate layer of the footwall compartment and then back into the same media in the hanging wall compartment (blue ray path **Figure 2.8**). This assumption is in agreement with Fermat's principle.

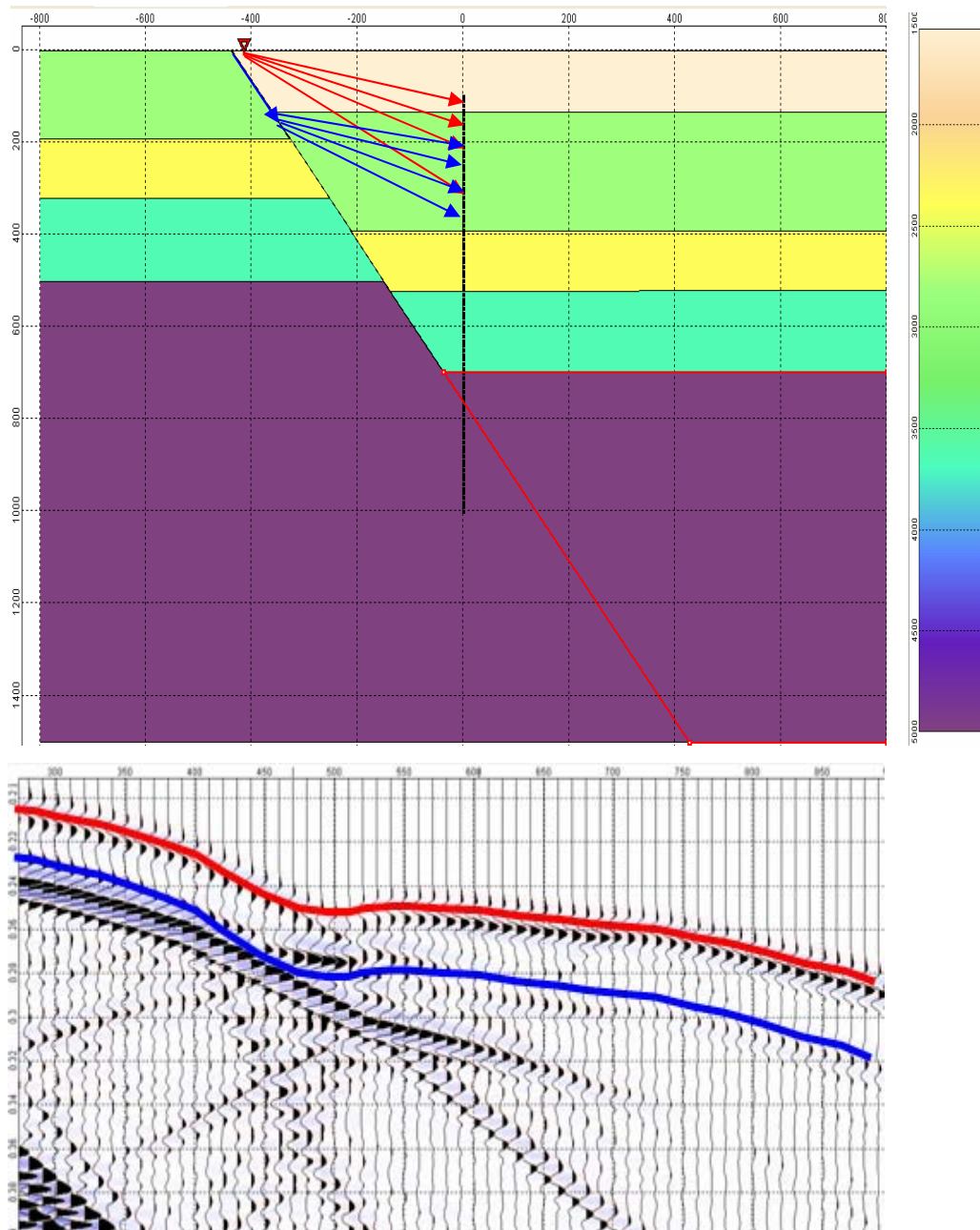
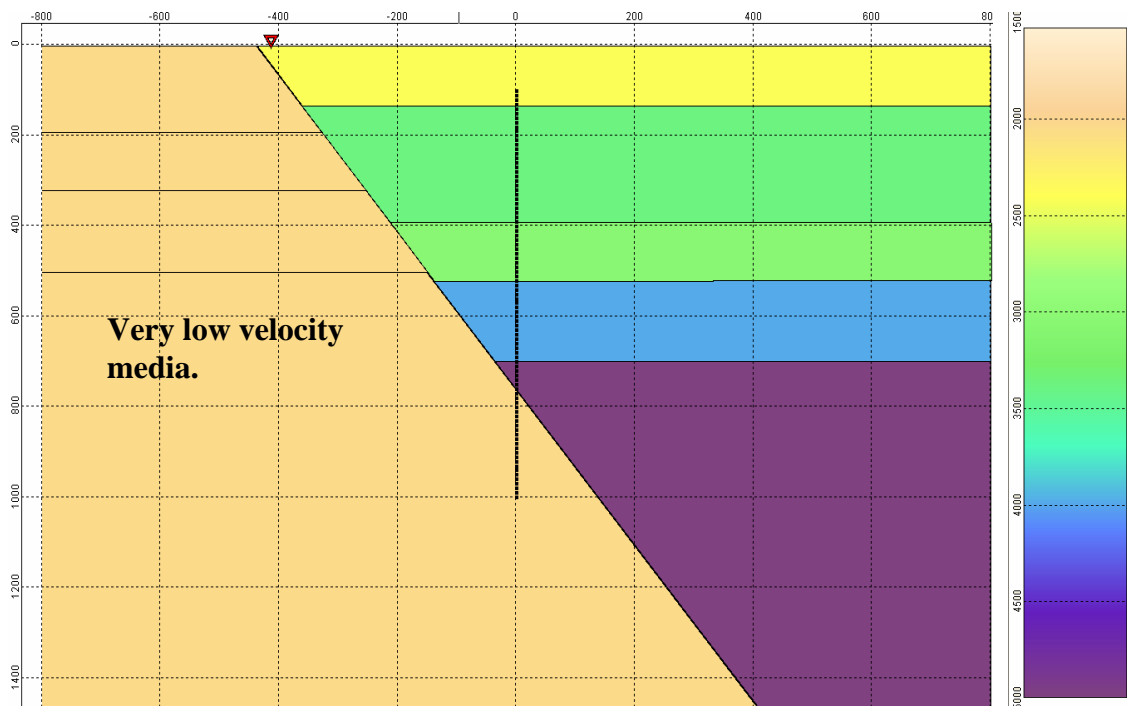


Figure 2. 8: Identification of the double direct arrival.

In addition, we note many hyperbolic patterns testifying diffraction events at the sharp corners created by the fault. The complexity of the generated seismograms prevents from accurately relating the observed events to their geological origin.

In order to check the assumption made justifying the double direct arrival we built a model where the entire footwall compartment was set to have very low constant velocity (Model 2. **Figure 2.9**). The generated results substantiate the wave behaviour in presence of high velocity layers (Fermat principle).

Model 2:



Elastic vertical component

Elastic horizontal component

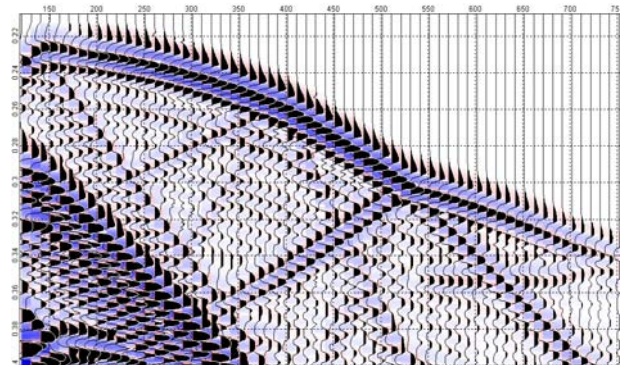
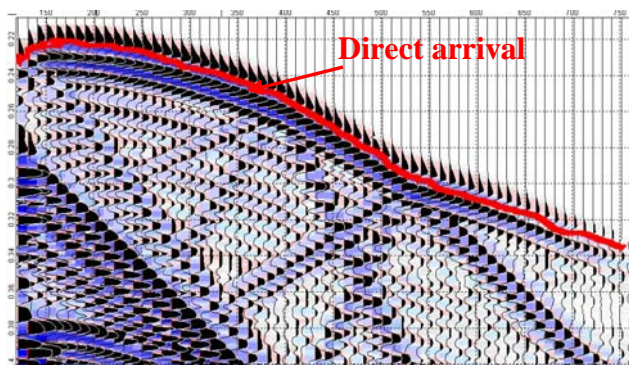


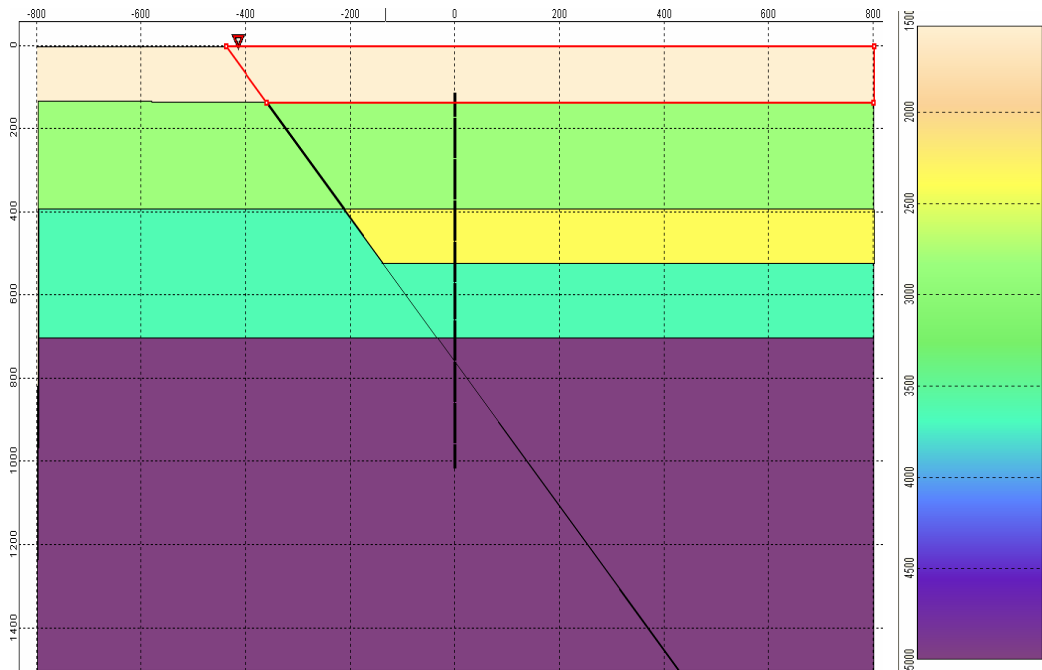
Figure 2. 9: Model 2 and the generated seismogram (Elastic vertical and horizontal components): we note that no fast arrival comes earlier than the direct arrival

The generated seismogram (**Figure2.9**) exhibits no arrivals preceding the direct arrival, which confirms the interpretation made in Model 1 stating that the early arrivals fit with Fermat principle and propagate along the highest velocity layers of the footwall compartment. The arrival time of the direct arrival in model 2 matches the arrival time of the “red-coloured” wave in the precedent model 1 (**Figure 2.8**).

The complex wave field in the fault vicinity, generated in the first model (Model.1 **Figure2.7**), has to be simplified in order to get relevant information. Therefore, we will simplify the previous model by building an intermediate model where we keep a 1D structure at shallow depth as if the fault does not exist. We just create a discontinuity (388m to 520m) by setting the clay layer of the hanging wall in contact with radiolarite and platy limestone layer of the footwall. By so doing we cancel the abrupt velocity contrasts along the fault plane creating diffracted waves which are absent in the field data, and we delete the double direct arrival that complicated the seismogram analysis at shallow depth.

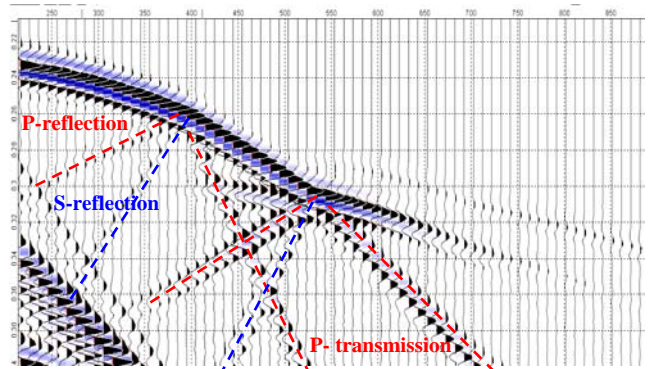
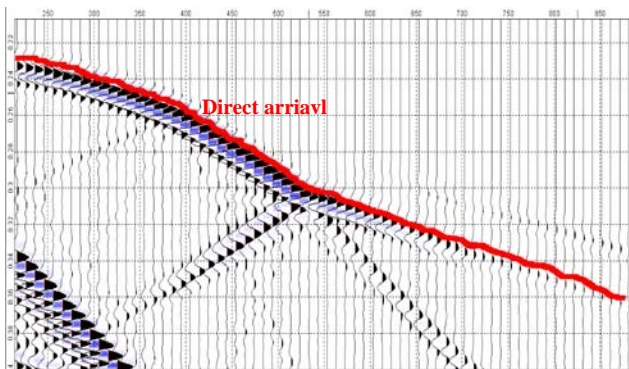
The resulting simplification on model 3 (**Figure2.10**) is justified by the fact that no early arrival is observed on the field data (**Figure2.5**), due to the presence of a fractured corridor along the fault that totally attenuates the seismic wave transmission between the hanging wall and the foot wall at shallow depth.

Model.3:



Elastic vertical component

Elastic horizontal component



Acoustic vertical component

Acoustic horizontal component

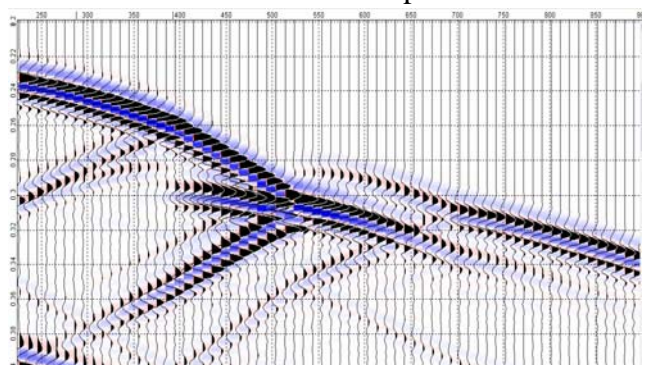
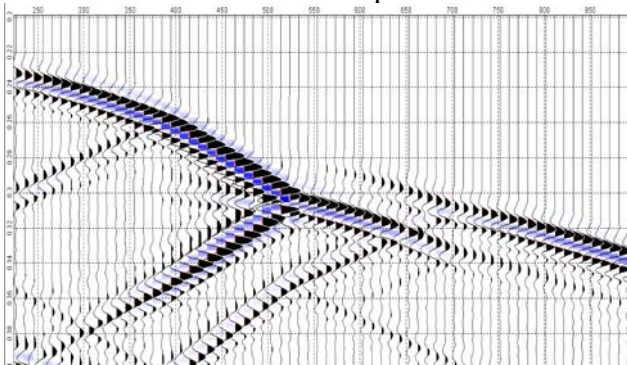


Figure 2. 10: Model 3 and the generated seismogram: Elastic and Acoustic vertical and horizontal components,

Observations:

✓ **Diffraction apex around 388m depth level.**

This model exhibits complex hyperbolic profiled signal with an apex at 388m, which attests the diffraction generated by the corner between the conglomerate, clay and the alternating radiolarite and platy limestone layers.

This hyperbolic pattern exhibits two branches (**Figure 2.11**):

- A fast upgoing signal ;
- A slow downgoing signal.

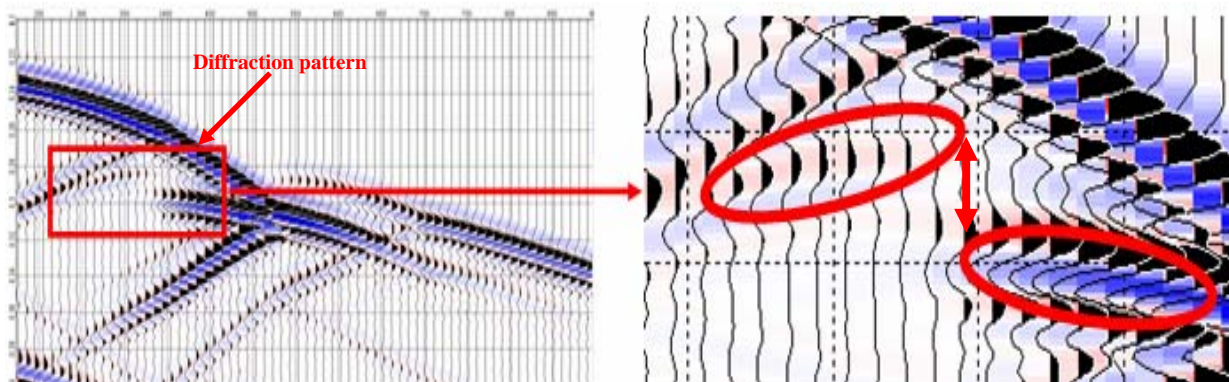


Figure 2. 11: diffraction pattern exhibiting an upgoing fast branch and a downgoing slow branch

This observation confirms the presence of a diffracted event at 388m corner. In fact the incident wave hitting the corner splits into upgoing signal that travels across the low velocity clay layer (2350m/s) and downgoing signal that travels across the higher velocity layer of conglomerate (2800m/s) (**Figure 2.14**).

The comparison of the horizontal and vertical components shows (**Figure 2.12, A and B**):

- An identical phase for the upgoing and downgoing waves in the horizontal component;
- An opposite phase for the upgoing wave and the downgoing wave in the vertical component.
- Higher amplitude in the horizontal component than in the vertical one.

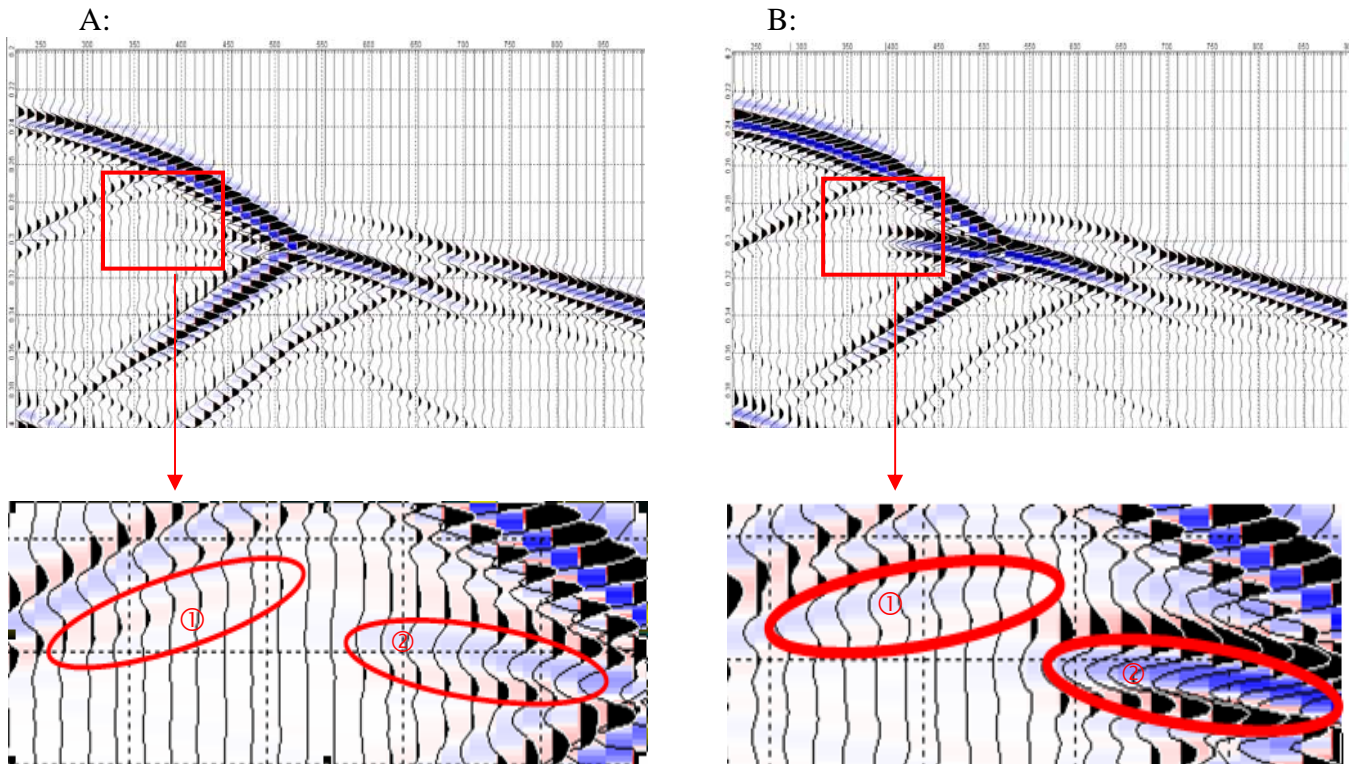


Figure 2. 12: **A:** vertical component (positive upgoing signal and negative downgoing signal),
B: horizontal component (negative upgoing and downgoing signal).

The last observations related to the diffracted signal phase leads to identify the following incidence of the diffracted waves: **(Figure 2.13)**

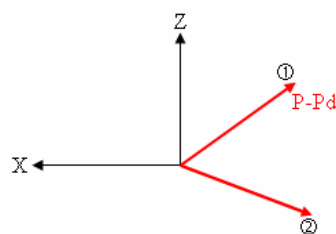


Figure 2. 13: incidence of the diffracted wave: ① upgoing diffraction branch, ② downgoing diffraction branch

The high horizontal amplitude compared to the low vertical one (Polarisation in the direction of propagation), combined with the fact that no major difference is seen between acoustic and elastic seismogram at the [0,26s; 0,3s] time range implies that the observed event is a P wave diffraction.

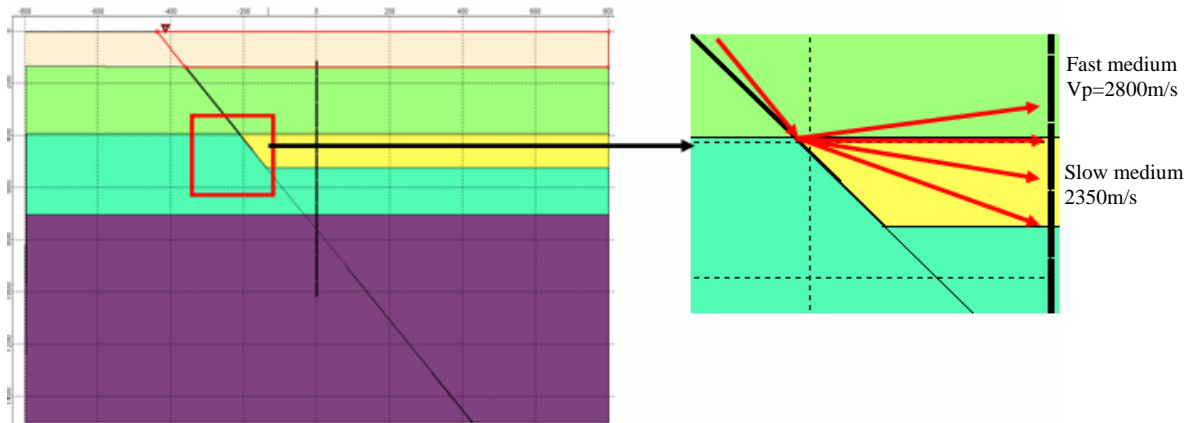


Figure 2. 14: Diffraction on the corner at 388m depth: the diffracted wave splits into an upgoing branch crossing the conglomerate layer (2800m/s) and a downgoing branch crossing the clay layer (2350m/s).

✓ **Diffraction apex around 520m depth.**

The second important event generated by model 3 is a hyperbolic pattern with an apex around 520m (**Figure2.15.top**). This pattern exhibits a time difference between the upgoing branch and the downgoing branch which attests the fact that the two branches travel through two different media (**Figure 2.15.bottom**).

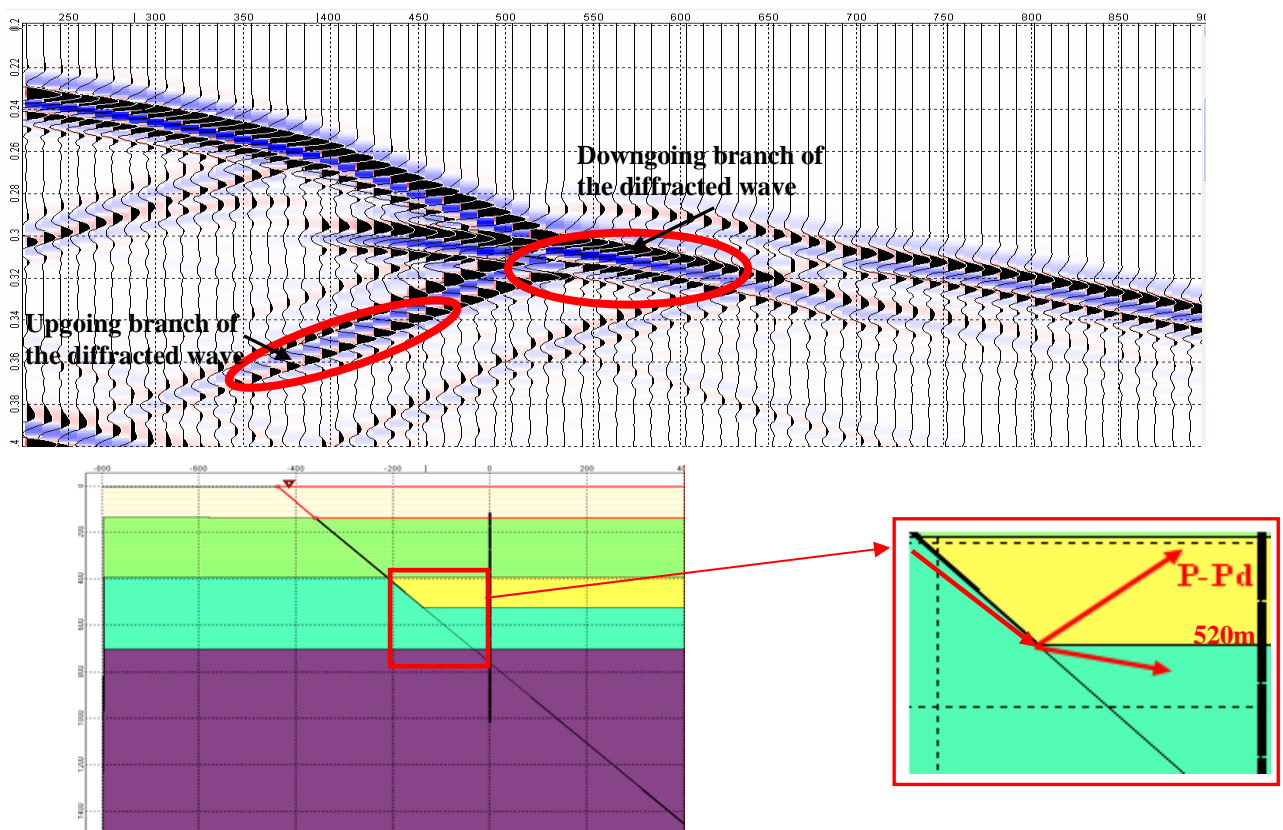


Figure 2. 15: Diffraction at the 520m depth corner. **Top:** Diffraction seismogram with apex around 520m,

Bottom: upgoing and downgoing branches of the Diffracted wave

Surprisingly, this signal is different from the observed hyperbolic profile seen in the field VSP data at 520m (**Figure 2.5**) as it is observed earlier than the direct arrival, just as the recorded diffraction observed on the real VSP data. In matter of arrival time, the diffraction apex of the real VSP data appears at 320ms versus 283ms in the synthetic seismogram (**Figure2.16**). This implies that the wave incident to the fault corner travels in a slower compartment than the modelled one.

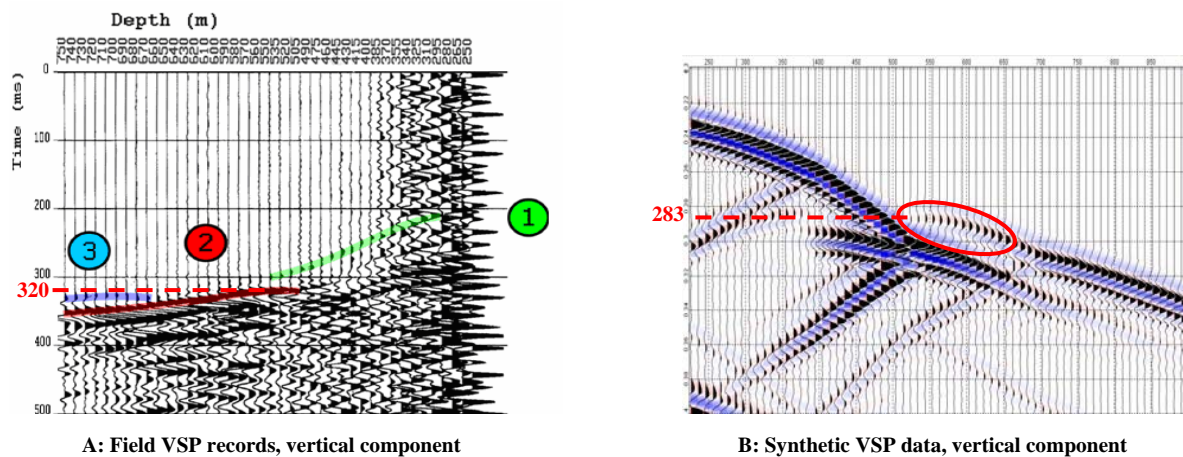


Figure 2. 16: 520m diffraction event time difference between: A. the recorded real VSP data and B. the synthetic model seismogram

On the model 3, the diffraction is likely to originate from an incident wave propagating through the high velocity alternating radiolarite and platy limestone layer (3600m/s) in the footwall hitting the 520m depth level fault corner, as illustrated on **Figure2.15**.

As the proposed model 3 does not exhibit the 520m apex diffraction like the one recorded in real VSP data (earlier arrival and weaker amplitude), modifications need to be made in order to match the arrival time of the observed events to the field VSP data.

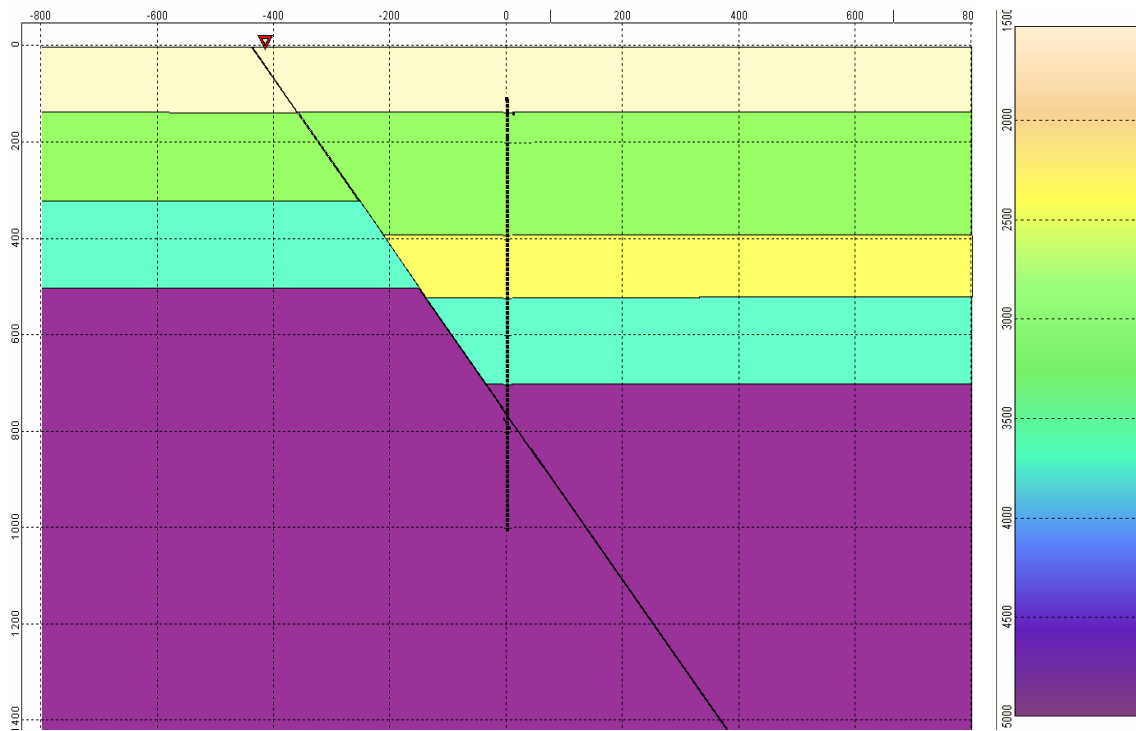
Summary of observations in Model 3:

Model 3 (**Figure2.10**) is a simplified cross section of the Aigion fault where we kept a 1D structure at shallow depth in order to cancel the double direct arrival unobserved in the field data. The generated seismogram exhibits diffraction events at the fault corners (520m and 388m depth). The investigation of these events (incidence, polarisation, phase and arrival time) allows identifying their origins and traveling paths. Mainly, we notice a diffraction apex around 520m depth that looks like the 520m depth diffraction apex seen in field VSP data. In

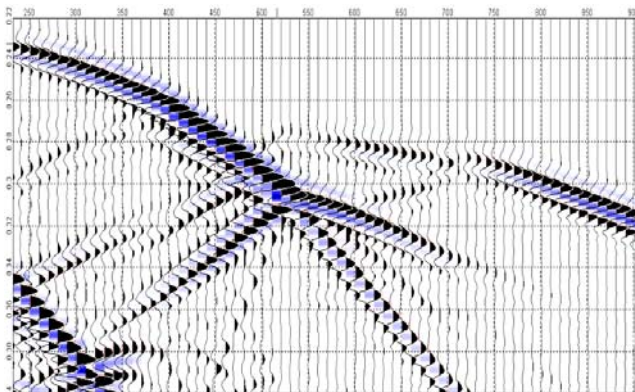
matter of arrival time, the diffraction events in the synthetic seismogram appear 37ms earlier than in the field data, implying that the incident wave actually propagates in a slower media than the modelled one (**Figure2.15**).

Model 4:

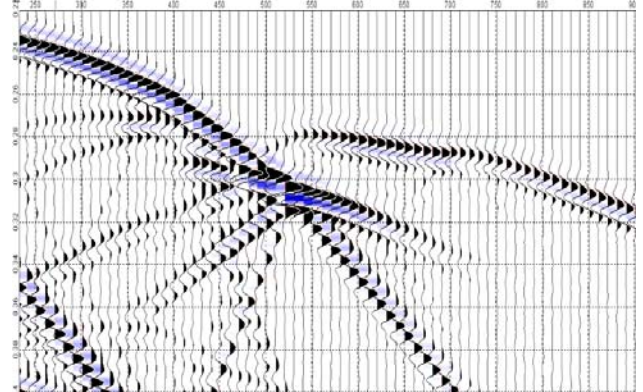
By respect to the fault throw value of 200m (*Place and al.2005*), we will shift the footwall's compartment layers upward. The radiolarite and platy limestone layer top will be positioned at 320m depth in the footwall and the carbonate layer's top at 500m. We will keep the 1-D shallowest layers structure in order to simplify the generated seismogram by deleting any unobserved early arrival.



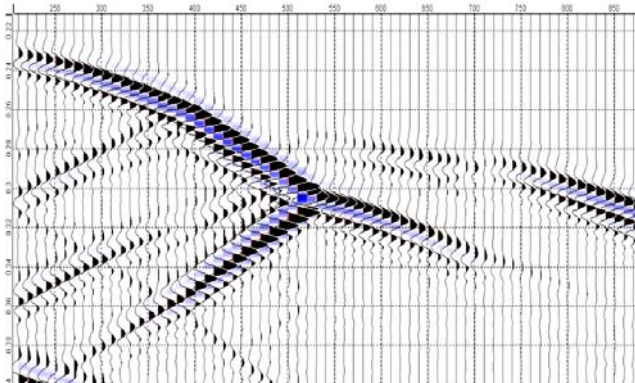
Elastic Vertical component



Elastic horizontal component



Acoustic vertical component



Acoustic horizontal component

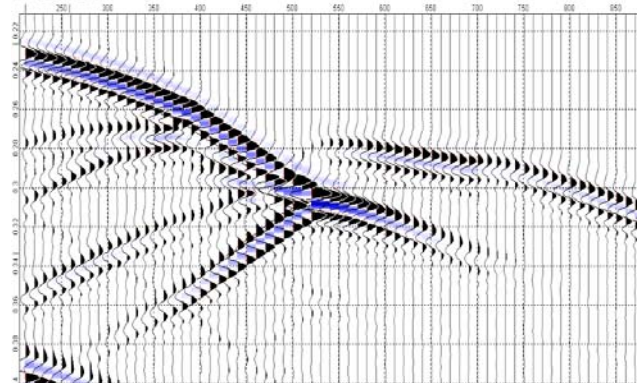


Figure 2. 17: Model 4 and the generated seismogram: Elastic and Acoustic vertical and horizontal component.

The model outputs reveal newly created signals due to the presence of the new fault corners.

Observations

✓ **Diffraction pattern around 320m depth.**

The seismogram reveals a hyperbolic wave pattern with an apex around 320m attesting a diffracted event on this corner. The downgoing branch of the diffracted pattern is not visible because of the interference with other seismic events having higher amplitude.

This diffracted wave has higher amplitude in the horizontal component than it is in the vertical one. Moreover it is detected in both the elastic and acoustic generated seismogram which testifies that it is P-Pd wave mode diffraction.

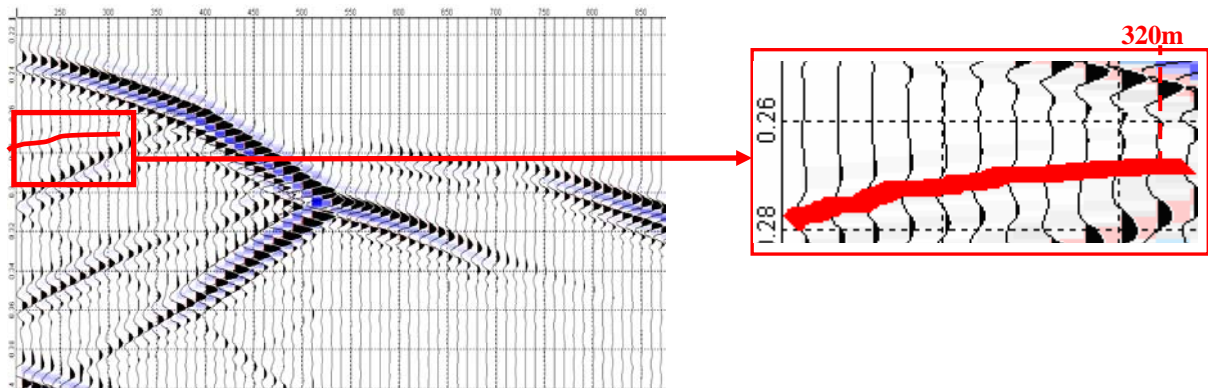


Figure 2. 18: diffraction pattern with an apex around 320m depth

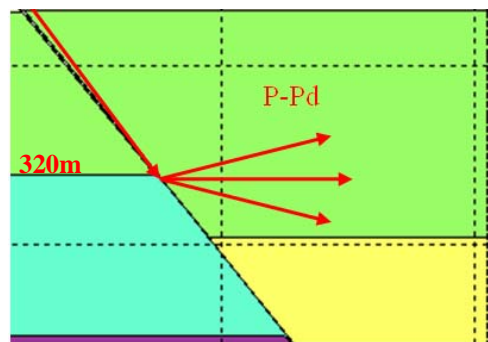


Figure 2. 19 : P-Pd diffraction at 320m depth corner

✓ **Late diffraction pattern around 388m depth:**

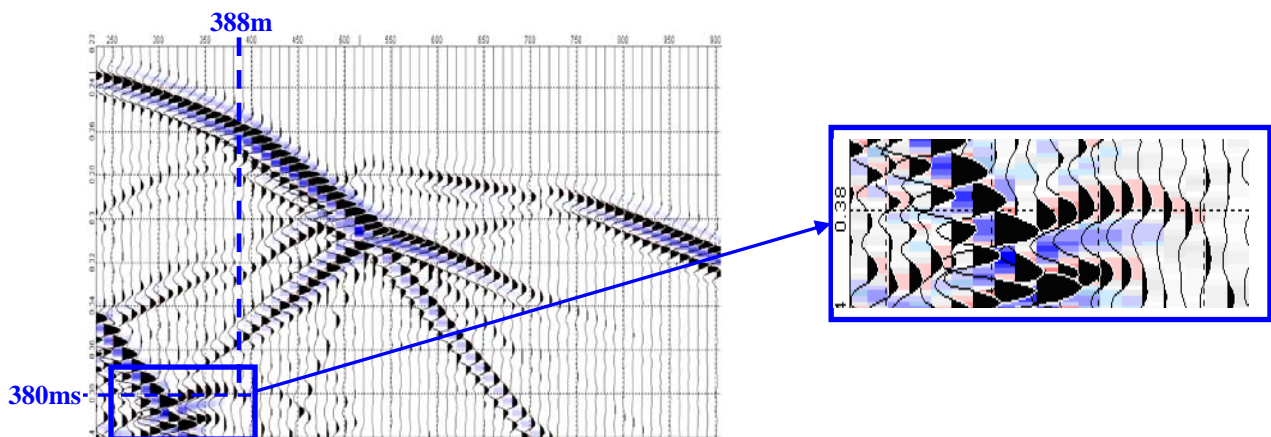


Figure 2. 20: P-Sd diffracted pattern having an apex around 388m.

The vertical component exhibits a diffraction pattern around 388m appearing around 380ms (later than the P-P diffraction pattern shown in **Figure 2.11**). This event is mainly observed in the vertical component and it is absent in the acoustic seismogram which attests a P-S diffraction (polarisation orthogonal to the propagation direction)

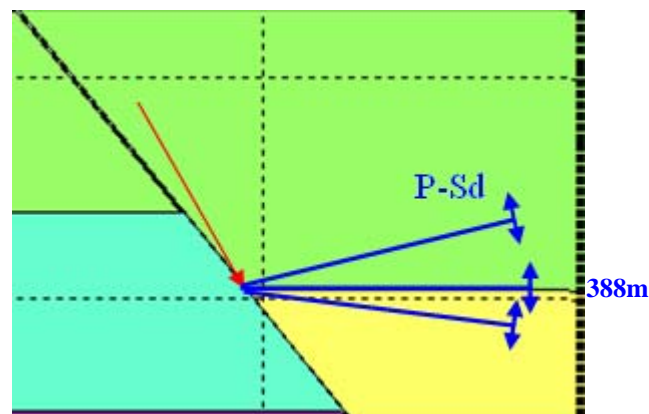


Figure 2. 21: P-S diffraction on the 388m depth corner.

✓ **Refraction pattern beyond 520m.**

The fact that we shifted the top of the carbonate layer in the footwall upwards to 500m shifted the wave coming before the direct arrival except around the 520m apex (**Figure 22**). In fact, comparing the first arrival time around 650m, for example, shows that the generated signal in the Model 4 arrives 10s earlier than the generated signal in model 3. Moreover, the diffraction hyperbolic profile's shape clearly observed in the Model 3 seismogram (**Figure 2.10**) was modified. In fact the diffracted downgoing branch presents a linear profile beyond its apex.

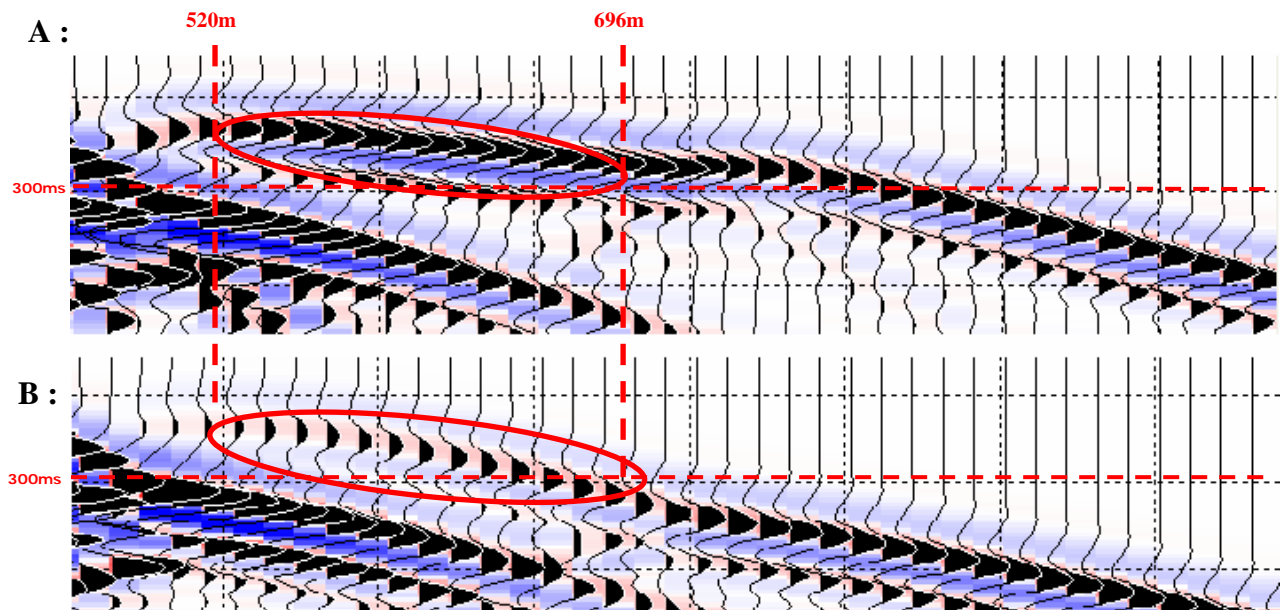


Figure 2. 22: A. Modified diffraction pattern in the model 4 seismogram having a quasi linear shape; B. clear hyperbolic diffraction profile in the model 3 seismogram.

These observations link this signal to a refraction event along the carbonate fault wall. In addition, an arrival time calculation (**Figure2.22**) reveals that the modification introduced in Model 4 shortened the observed signal at 700m depth as it appears 17ms earlier than in the Model 3. This remark agrees with the time difference between the diffraction and refraction events observed in field data and calculated in previous works (*Place and al. 2005*)².

This refracted wave is likely to accounts for the observed propagation along the carbonate layer of footwall compartment described in real VSP data (Wave (3) in **Figure2.5**) but it differs by its arrival time. In fact, the generated refraction in the synthetic seismogram appears 45 ms earlier than in the real VSP records. This observation testifies the fact that the refracted wave, generated in this model, doesn't travels through the hanging wall compartment after encountering the carbonate fault corner (520m). But it originates from an incident wave propagating entirely in the hangingwall compartment prior to encountering the carbonate fault corner. This observation mismatches the previous assessments of waves travel path (*Place and al .2005*).

² An arriving time difference calculation revealed a 20ms time difference between the recorded diffraction and refraction events.

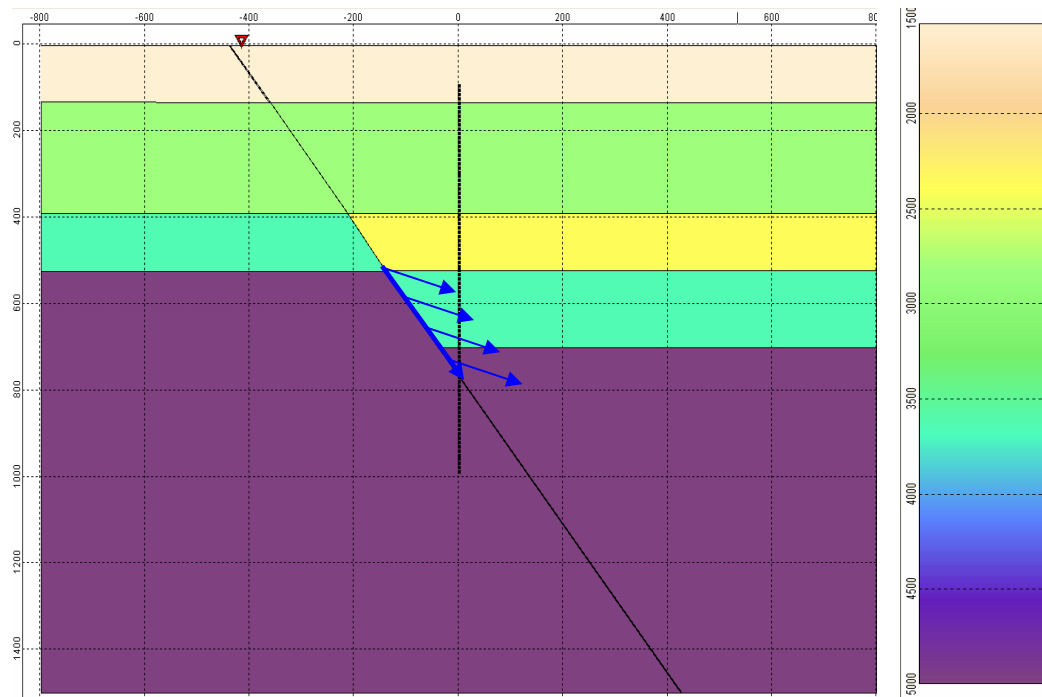


Figure 2. 23: Refracted wave upon the carbonate layer wall.

Summary of observations in Model 4 :

In Model 4 we shifted the footwall compartment layers upwards by respect to the fault throw (200m). This modification generated additional diffraction events at the newly created fault corners (P diffraction at 320m and S diffraction at 388m). Mainly, this model explains the early linear wave pattern appearing beyond 520m depth as a refraction event along the carbonate layer wall. In a matter of arrival time, the refracted wave exhibited in the synthetic model appears 45ms earlier than in field VSP data.

In order to summarise, through the precedent modification steps we explained the major seismic events that we noted in the first synthetic model (Model 1 **Figure2.7**). The generated seismograms exhibit arrivals that are representative of the real signals but they differ in terms of arrival times which are shorter: according to Fermat principle they travelled through the higher velocity footwall compartment.

The field VSP data do not reveal waves arriving as early as the signals generated in the synthetic seismogram of model 4 and 5 (the diffraction at 520m depth and the refraction along the carbonate layer of the footwall). A possible explanation for this oddity could be that the fractured and heterogeneous nature of the earth in the fault vicinity attenuates waves going across the fault zone to the high velocity media of the footwall compartment. Thus, after

examination of the possible causes of this difference with respect to the real VSP data, we intend to introduce attenuated geological bodies in order to correct the suggested models and reproduce more accurately the major events observed on the real VSP's.

2.3. Correction of the fault model sketch using the attenuation effects:

The step by step modelling approach that we used helps understanding the complex generated seismogram and relates the major observed events to their originating causes. Mainly, we have confirmed the origin of the early signals that reach the receivers before the direct arrival. These arrivals, as explained in preceding models, testify the propagation of seismic waves in high the velocity media of the footwall compartment (higher than those crossed by the direct arrival on the hanging wall compartment). The presence of these early arrivals complicated the generated seismograms and rendered the accurate identification of the arrivals (1, 2 & 3 **Figure 2.5**) observed on the real VSP records more difficult.

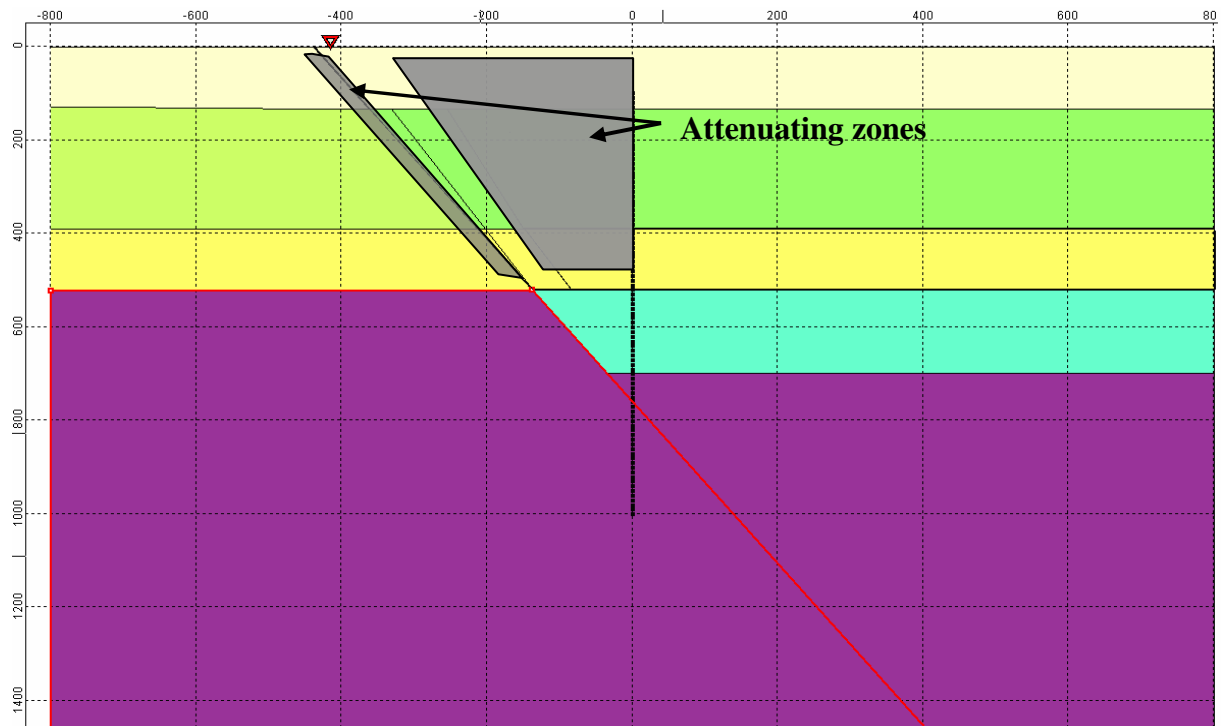
The fact that field recorded VSP data do not exhibit these early arrivals leads to the assumption that a highly fractured zone distributed along the fault attenuates the seismic waves and prevents them from crossing the fault zone into the faster medium in the footwall compartment and at shallow depth.

In order to justify the above hypothesis and to circumvent these oddities we suggested setting a fractured zone in the fault vicinity (**Figure2.24**). For a reason of simplification, we will use the model where the shallow part is set to have 1D structure as we intend to focus on the deeper events. This attenuating fractured zone was positioned in a manner that it prevents any wave transmission across the fault toward the footwall compartment.

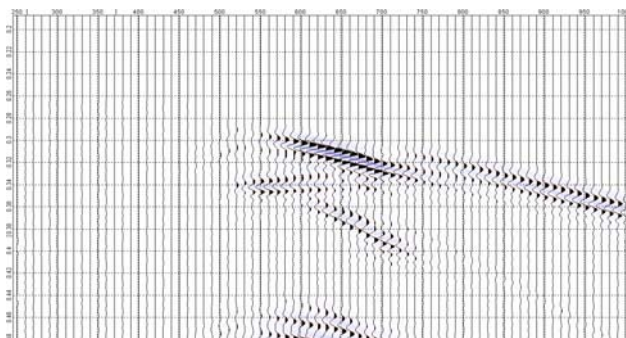
Moreover, the location and shape of the fractured zone located between VSP3 and the well was based on the examination of the weak amplitude of the direct arrival observed in real VSP data and on the propagation paths proposed in the previous publication (*Place and al. 2005*). In fact, the fractured zone, expected in the fault vicinity, attenuates only the direct arrival as it loses energy in the shallow layers. The diffracted wave (2), seen in real data (**Figure2.5**), exhibits almost the same amplitude which testifies that it does not travel across the highly attenuating zone. So we shaped this zone in a manner that only the direct arrival (1) travels through it.

2.3.1. Investigation of VSP3:

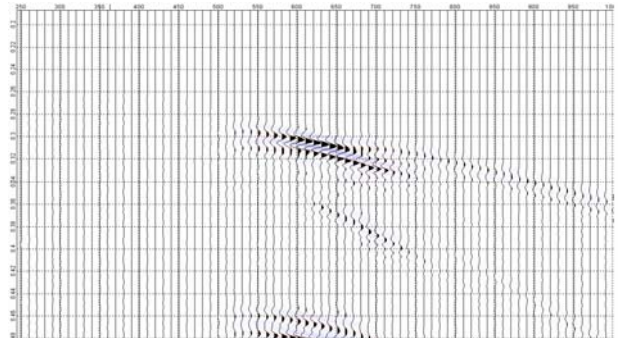
Model 5:



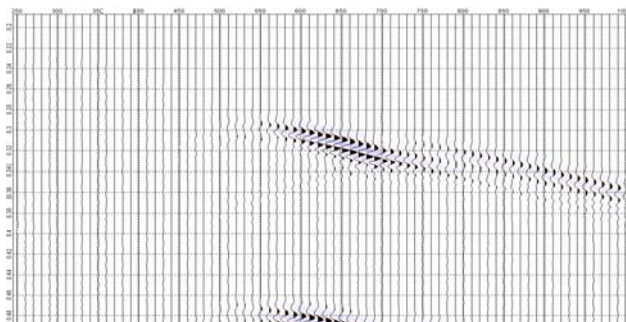
Elastic vertical component



Elastic horizontal component



Acoustic vertical component



Acoustic horizontal component

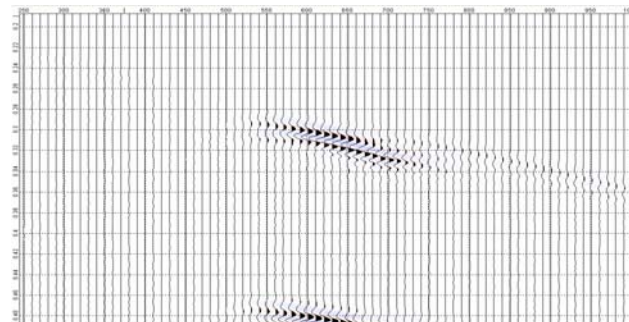


Figure 2. 24: Model 6 and generated seismogram: This model includes an attenuating zone in order to reproduce the real VSP major events.

As expected, the attenuating zone added to the model faded out the fast direct arrival that precedes the observed arrivals. Thus, we clearly identify a signal exhibiting a linear slope starting around 600m which matches the refracted wave detected in the real VSP data (wave 3 **Figure2.5**). This wave emerges under critical refraction from the tectonic contact between limestone and radiolarite in the depth interval 500-696 m.

In addition, we identify a hyperbolic pattern showing an apex around 520m. The arrival time of this diffracted wave matches the time of the diffracted arrival 2 (**Figure2.5**) on the real VSP data (~320ms apex time) (**Figure 2.25**).

The direct arrival exhibits the same behaviour in the synthetic seismogram as in the real VSP data: (see the amazingly reduced amplitude at all depths) which confirms the adequacy of the proposed model (**Figure2. 25**).

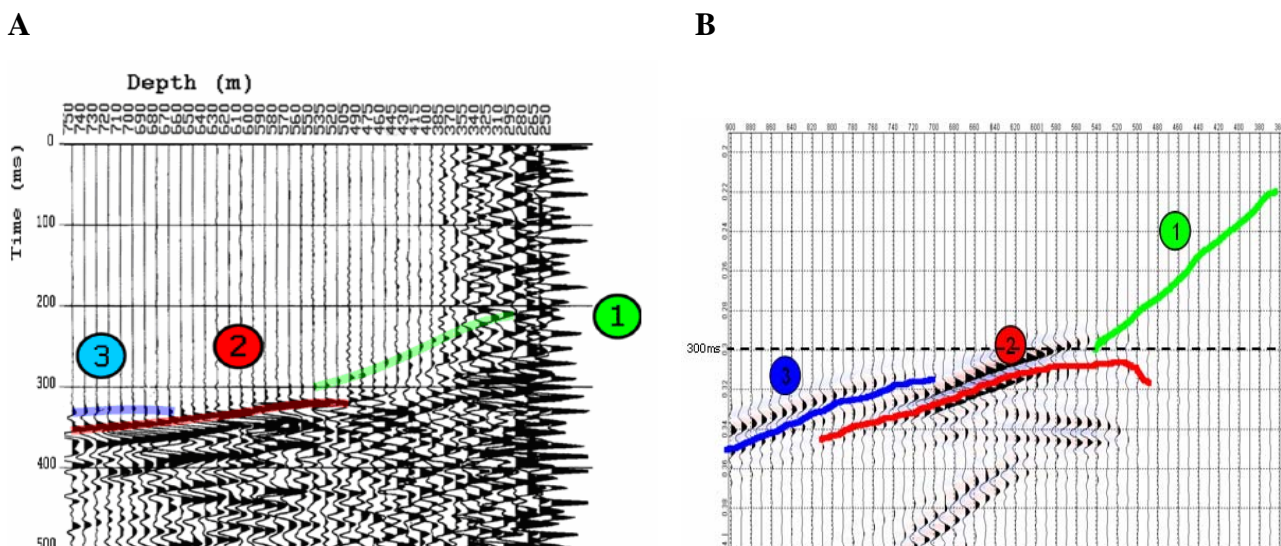


Figure 2. 25: Vertical component in both real VSP data (**A**) and the generated synthetic seismogram (**B**) of Model6 exhibiting the same major seismic events: (1) direct arrival, (2) diffracted wave 520m, (3) refracted wave.

The **Figure2.25** illustrates the comparison between the real VSP data and the synthetic seismograms. In fact, the proposed model is likely to reproduce the real wave behaviour in the fault vicinity and can be used to identify the origin of the different seismic events in terms of structural features in the well vicinity.

The following **Figure2.26** illustrates the identification of the different seismic arrivals through the geological structure of the AIGION fault resulting from the modeling approach.

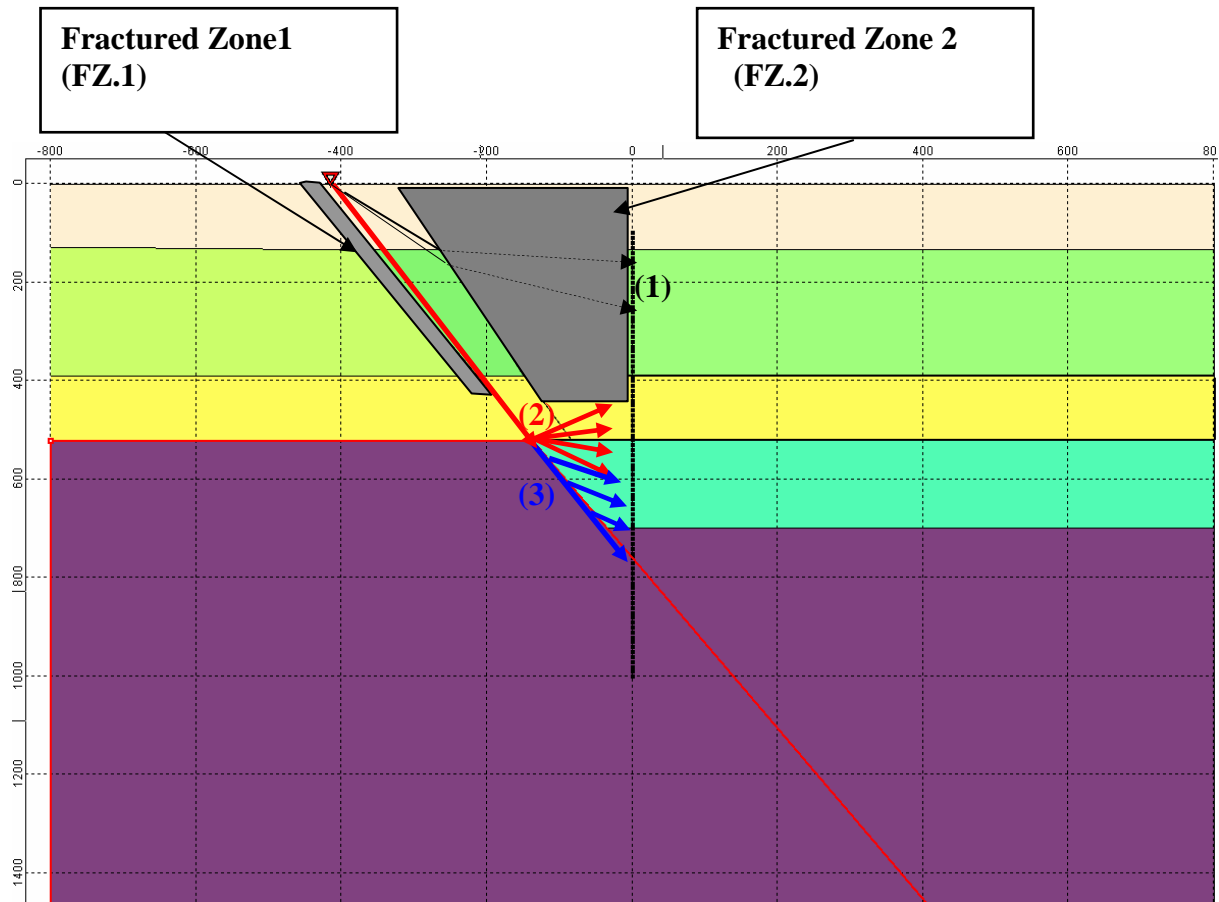


Figure 2. 26: Seismic paths in the fault vicinity: this figure shows the travel path identification of the waves seen in the real VSP data. (1) Direct arrival (highly attenuated), (2) Diffracted wave at 520m depth, (3) refracted wave along the carbonate layer.

The modelled seismograms match the real VSP data which improves the confidence in the structure of the fault vicinity.

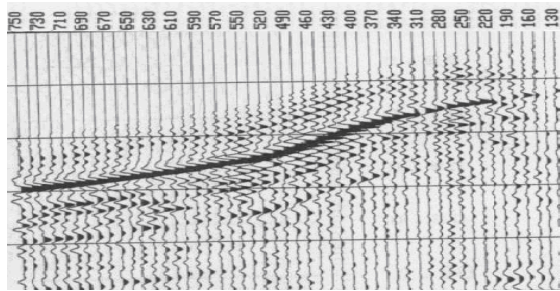
The 2D finite difference modelling procedure enabled to regenerate the main seismic events present in the real VSP data. In fact, through step by step modifications applied to the model we were able to imitate the real records. Mainly, this work unveiled the presence of attenuating fractured zones in the immediate vicinity of major faults and at shallow depth. The attenuating zones were identified and located by regards to their effect on the wave behaviour either in real VSP data or in the synthetic model.

To accurately identify the position of the detected fractured zone (FZ.2), located between the well and the Aigion fault, and refine its shape we will identify its effect on other VSP records: VSP6 and VSP1.

2.3.2. Investigation of VSP6:

To refine the shape and position of the fractured zone (FZ.2) we will investigate the VSP6 seismogram. VSP6 is an offset VSP located at 144m south of the well, at an intermediate position relatively to the Aigion fault. Although the source position is located right above the 520m depth carbonate fault corner.

A:



B:

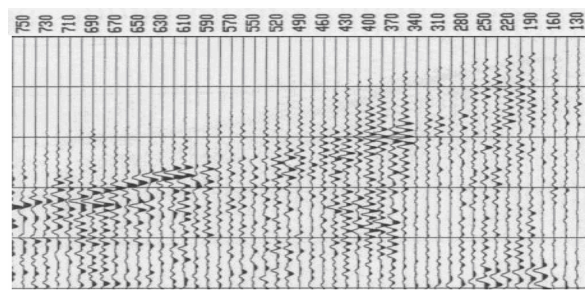
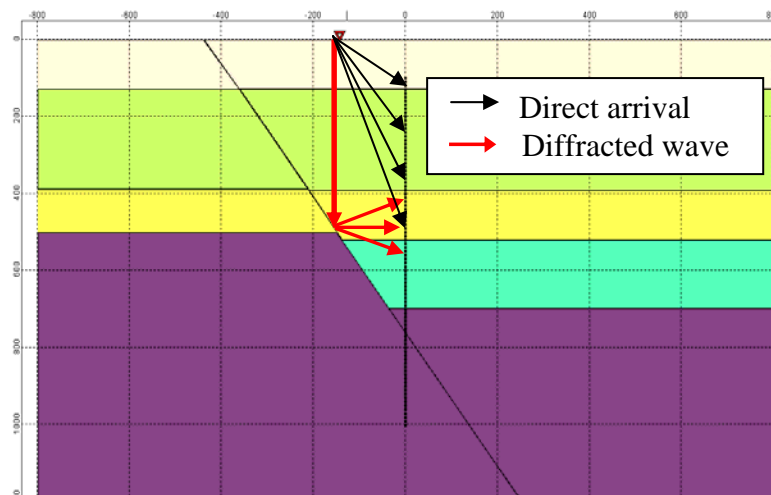


Figure 2. 27: Field VSP data: **A:** vertical component (Z) , **B:** horizontal component (HR).

The field data do not exhibit any diffracted event at 520m depth fault corner

Model 6:

This model illustrates the VSP6 in the geological cross section without adding the fractured zone FZ.2.



Vertical elastic component

Horizontal elastic component

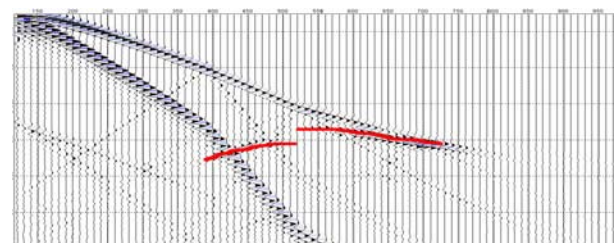
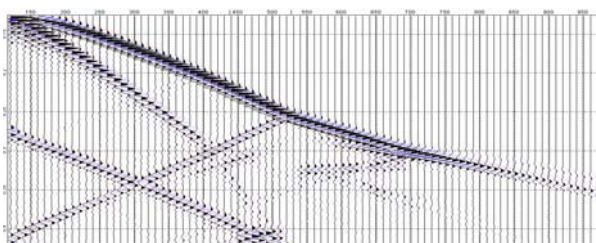
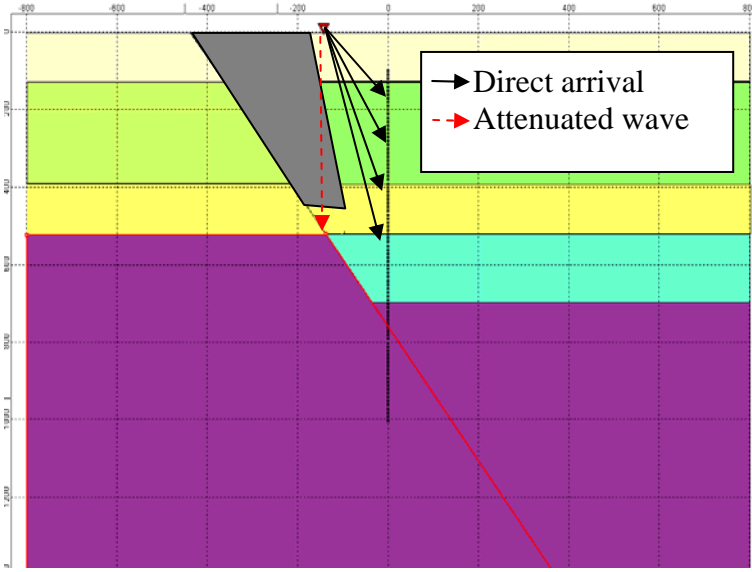


Figure 2. 28: VSP6 Model without the attenuating zone, note the presence of a diffraction apex at 520m depth (unseen in field VSP data).

The generated seismogram exhibits a diffraction pattern with an apex around 520m depth unseen in field data (Figure 2.28). This observation confirms the existence of the fractured zone that prevented the generation of any diffraction at the 520m depth corner between the Aigion fault and the well. To match the field data, we introduced the fractured zone in a manner that it cancels the diffraction at the 520m depth corner without affecting the direct arrival travel path recorded in the field data (Figure 2.29).



Elastic vertical component

Elastic horizontal component

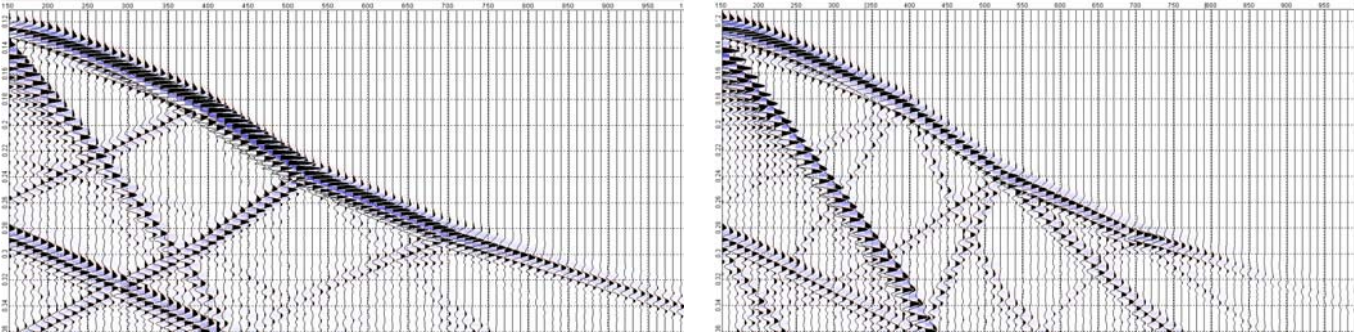


Figure 2. 29: Model 6 with the attenuation zone: VSP6 (144m offset) and the generated seismograms.

The generated seismograms do not exhibit any diffraction or refraction events. Only P-P, P-S reflection and transmission are observed (Figure 2.29). This synthetic model matches the real VSP6 data. This simulation will help positioning the attenuating zone.

2.3.3. Investigation of VSP1:

VSP1 is a zero offset VSP, through its investigation we intend to confirm the presence of the detected fractured zone FZ.2 and have an additional idea about its position. We start to simulate the Model without the fractured zone (**Figure2.31**). Then, we compare the generated synthetic seismograms with the field data (**Figure2.30**) and examine the difference. This process helps delineating the fractured zone.

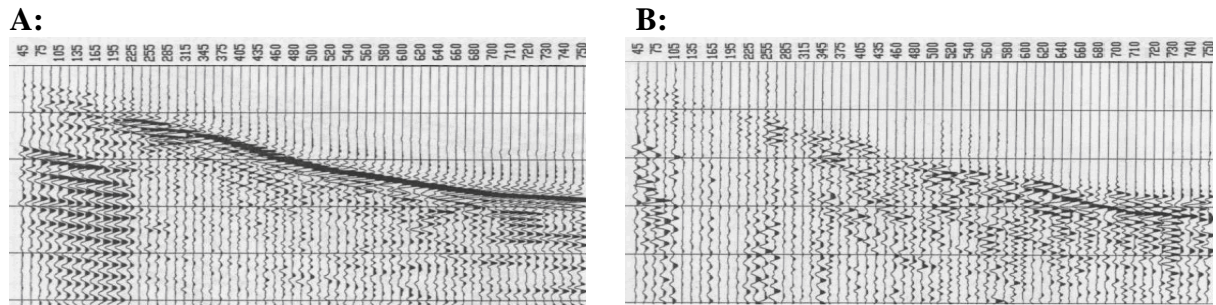
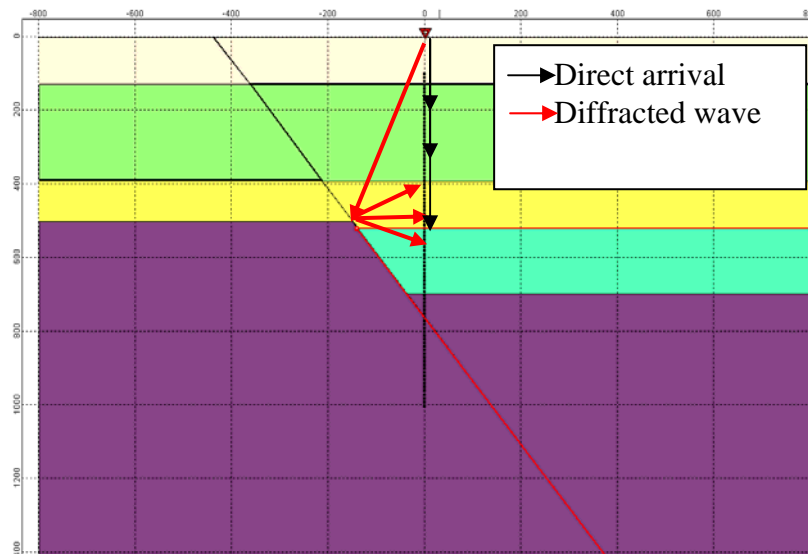
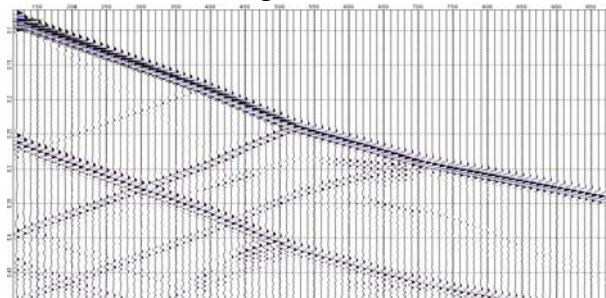


Figure 2. 30: Field data VSP 1 (zero offset): **A:** vertical component, **B:** Horizontal component

The field VSP data (**Figure2.30**) exhibit no particular event around 520m depth fault corner. We will compare this seismogram to the synthetic one generated by the following model.



Elastic vertical component



Elastic horizontal component

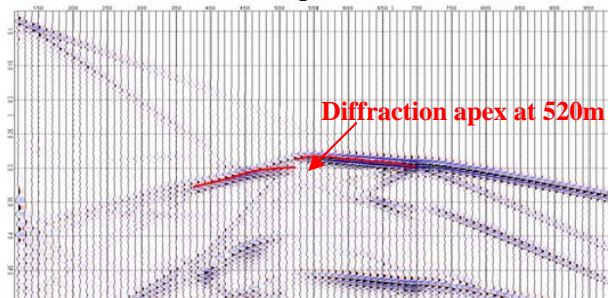
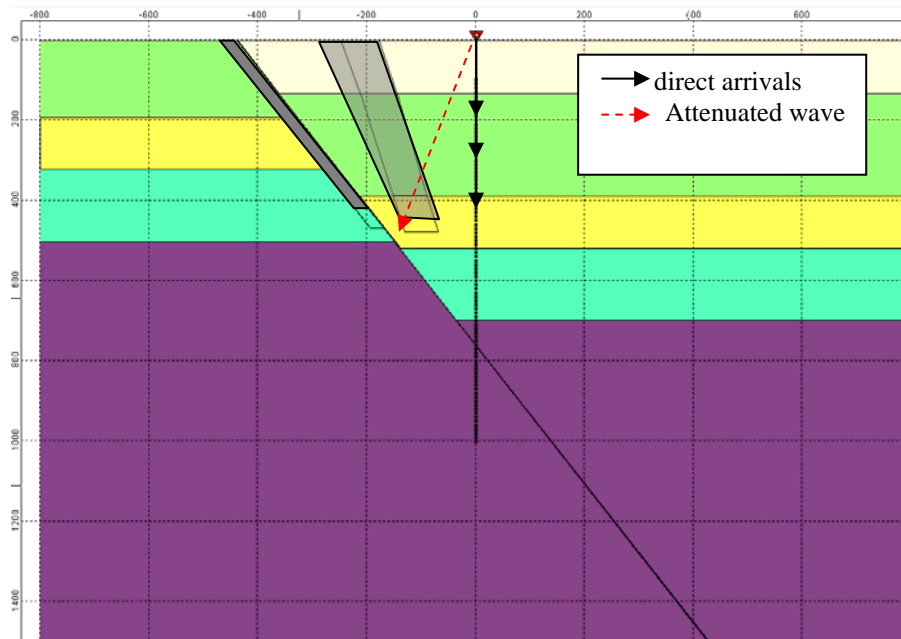


Figure 2. 31: VSP1 model without an attenuating fractured zone: note the presence of a diffraction apex at 520m unseen in field VSP data.

The synthetic seismogram exhibits a diffraction pattern at 520m depth (**Figure 2.31**). This event is unseen in the field data (**Figure 2.30**) which confirm the presence of a fractured zone situated between the fault and the well and attenuates the incident wave diffracted at 520m depth in the synthetic model.

In the following model we run the zero offset VSP with the fractured zones.



Horizontal component

Vertical component

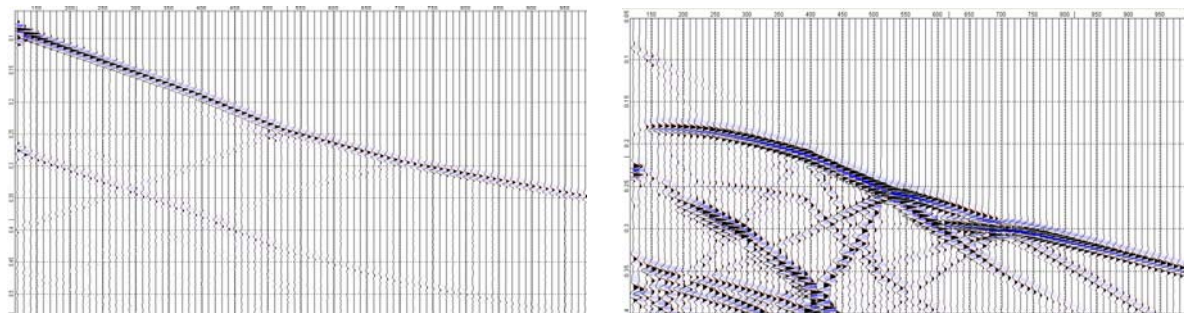


Figure 2. 32: VSP1 model with fractured zone FZ.1 and FZ.2: no diffraction apex is seen in the generated seismogram on the vertical component.

As expected the fractured zone added to the model deleted the diffraction pattern observed at 520m on the vertical component (compare with **Figure2.31**), in agreement with the field data. On the horizontal component, the new high amplitude events appearing above 520m are generated by reflection and diffraction on the attenuating FZ2 polygonal domain.

The combination of the VSP3, VSP6 and VSP1 models leads to accurately define the position of the attenuating zone (FZ.2) (**Figure 2.33**). FZ.2 seems to correspond to a secondary fault parallel to the main Aigion fault.

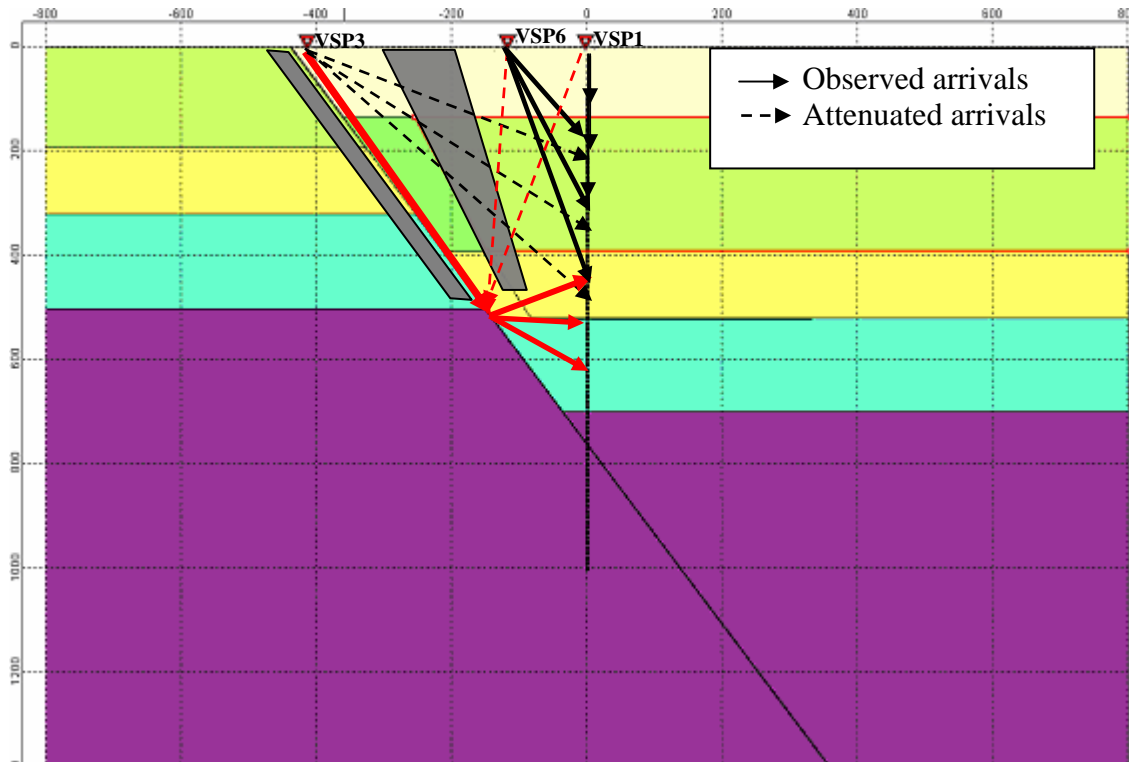


Figure 2. 33: Accurate position of the fractured zones and their effects on the wave propagation as revealed by the modelling procedure.

Once the position of the fractured zone was determined, we intend to check the effect of this zone (FZ.2) in the complete model (Model 1) that includes the real cross section of the Aigion fault without simplification (**Figure 2.34**).

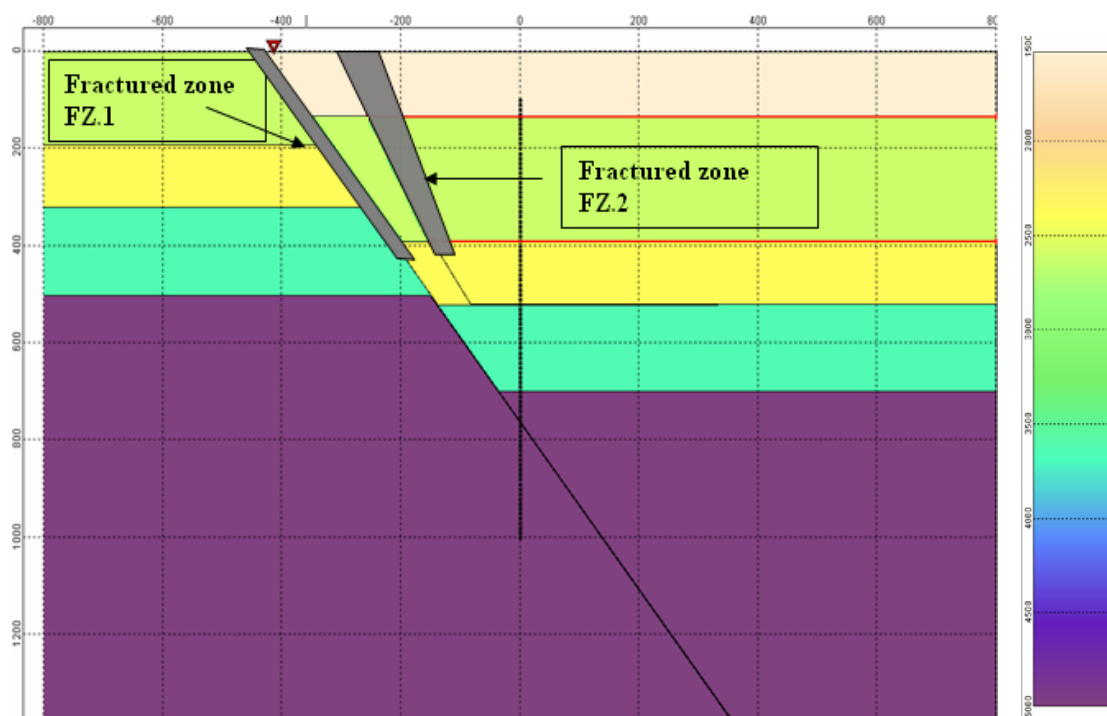
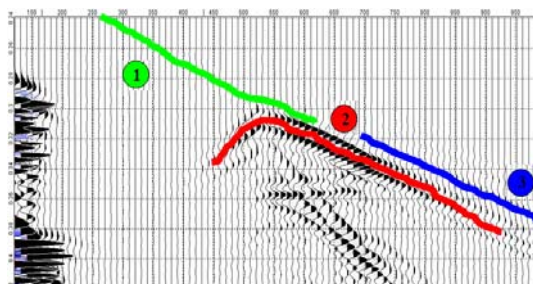


Figure 2. 34: The actual Aigion fault cross section corrected by adding fractured zones as revealed through the modelling procedure.

Elastic vertical component



Elastic horizontal component

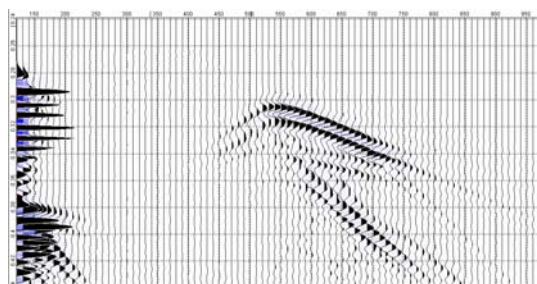


Figure 2. 35: Elastic vertical and horizontal component of the generated synthetic seismogram matching the real data recorded from VSP 3. (1): direct arrival exhibiting weak amplitude in shallow depths, (2): diffracted wave upon the 520m depth corner, (3): refracted wave upon the carbonate layer of the footwall compartment.

The generated seismogram (VSP3) compared to the field VSP 3 data exhibits the same main seismic events (weak direct arrival, diffraction pattern at 520m depth, and a refraction pattern: **Figure2.35**). This observation confirms the accuracy of the structural cross section model suggested in this work.

The attenuation effect is most probably caused by the fractured and decompressed nature of rocks in the shallow layers in the hanging wall compartment and along the Aigion fault. This fractured zone as shaped through the modeling looks like a secondary fault parallel to the main Aigion fault. The model sketch previously suggested to describe the Aigion fault (**Figure2.6**) has been refined by adding the fractured faulted zone (F.2) identified in the present study (**Figure2.36**).

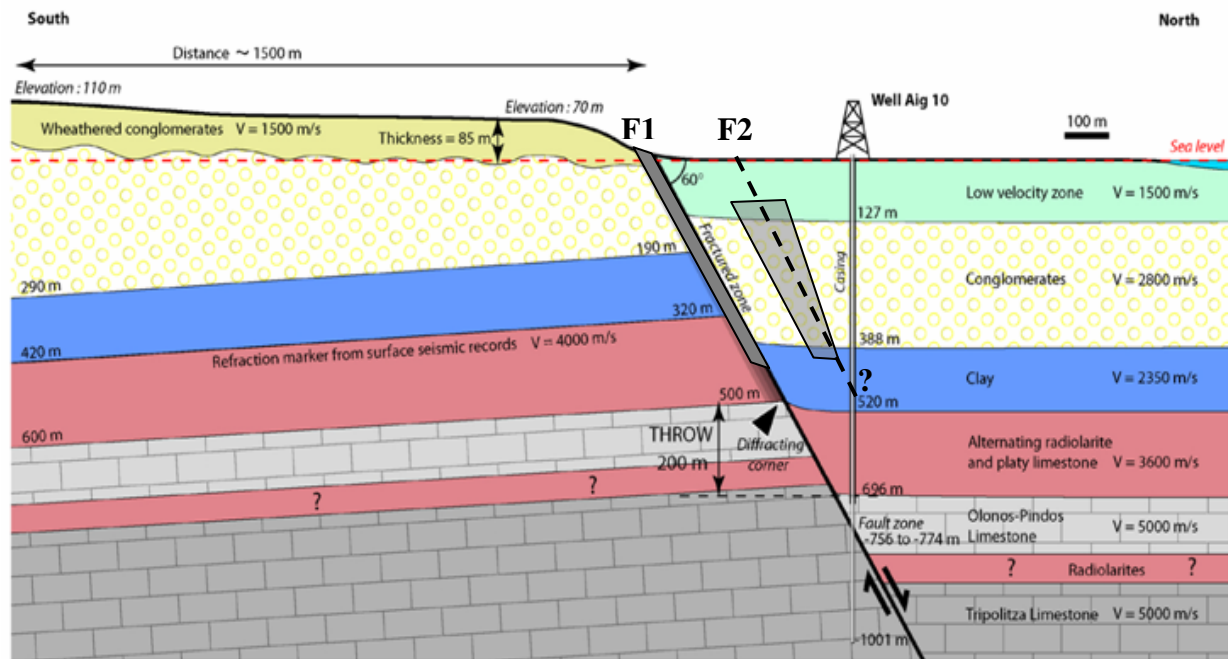


Figure 2. 36: Corrected velocity model of the Aigion fault vicinity: the present work allowed identifying a fractured zone between the well and the fault in shallow depths

2.4. Summary of the modelling procedure and the relevant results:

The present work was based on the reconstitution of the wave propagation through the geological structure of the Aigion fault vicinity. The gradual modifications applied to the built models and the investigation of the generated events (diffraction and refraction) allowed relating the obtained signal in the synthetic seismogram to their geological origins and defining their propagation paths.

In the first models built (Model 1, 2, 3 and 4) we obtained the major seismic events seen in field VSP data (event 1, 2 and 3 **Figure2.5**). But, the synthetic seismograms exhibit these events at earlier time than the field data (**Figure2.16** and **2.22**) which implies that they propagated in the high velocity media of the footwall. This difference reveals the existence of

fractured zones that totally attenuates the seismic propagation. Mainly, the reconstruction of the propagation path of the major seismic events in VSP3 unveiled the presence of a fractured zone situated between the Aigion fault and the AIG-10 well (FZ.2 in **Figure 2.26**). The investigation of VSP1 and VSP6 allowed accurately positioning the fractured zone and relating it to a secondary fault F2 parallel to the main Aigion fault (**Figure 2.33, 2.34 and 2.36**).

The presence of similar minor faults not involving the basement was confirmed by geologic observation of outcrops in the Aigion area.

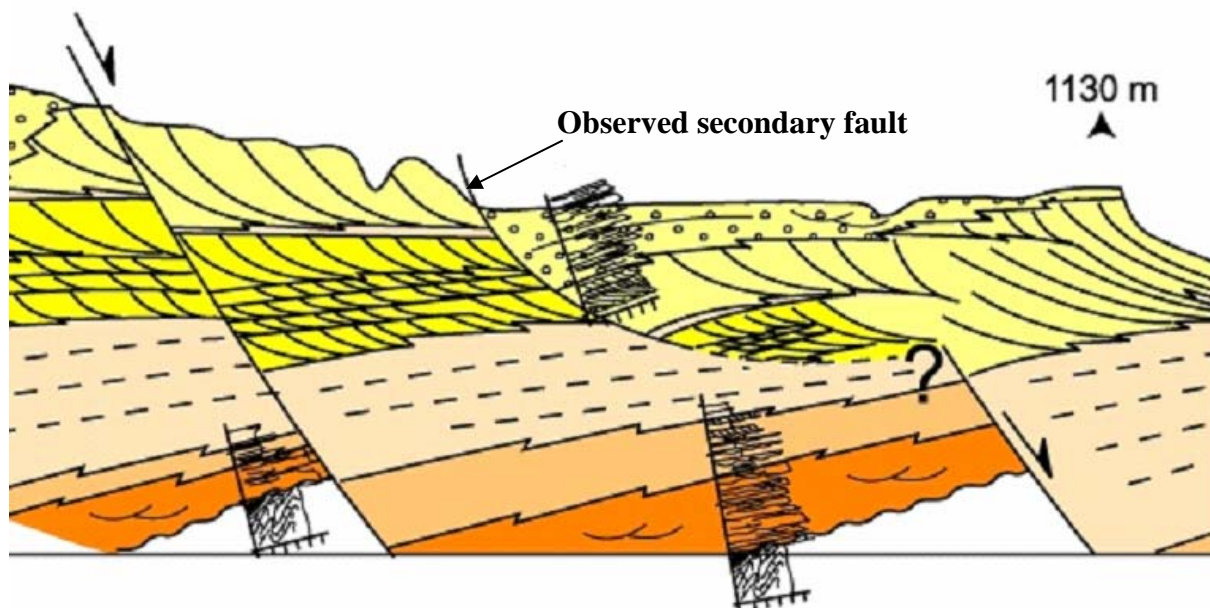


Figure 2. 37: Presence of a secondary fault in principle fault in the Gulf of Corinth area illustrating the presence of the detected secondary fault (*Rohais,2005*).

In the present paragraph we intend to find an element of explanation to the absence of reflection event in field data, in spite of the presence of a high velocity contrast in the Aigion fault vicinity. We suggested to model two media with a high velocity contrast. The interface between the two layers is rugged and exhibits sharp accidents. The resulted seismogram is compared to the result issued from a model with a horizontal interface between the two medium.

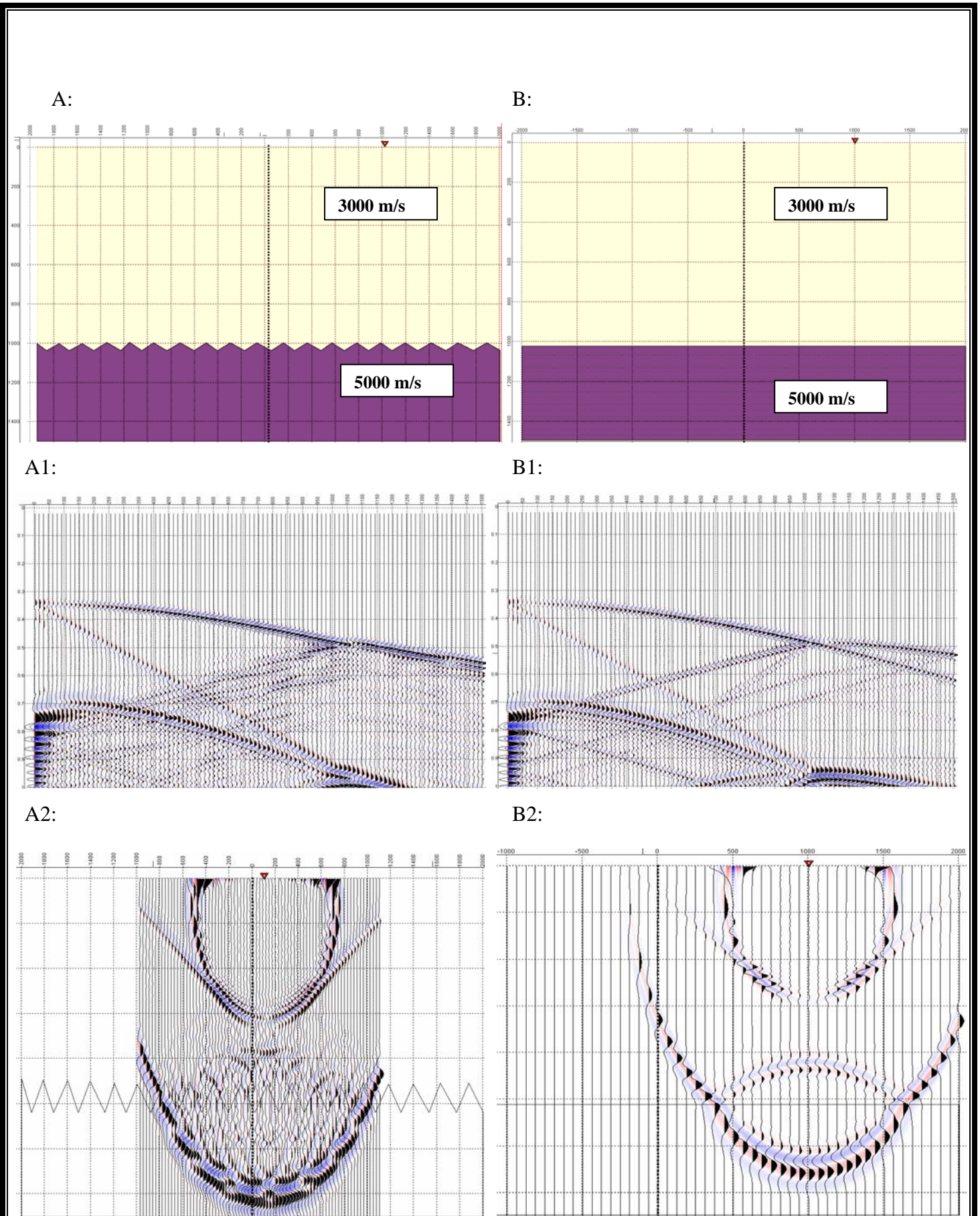


Figure 2. 38: A: high velocity contrast interface with a rugged surface. **A1:** vertical component seismogram .**A2** snapshot. **B:** high velocity contrast with horizontal surface.**B1:** vertical component seismogram, **B2:** snapshot

The comparison between the two models shows that the rugged interface generates a distorted reflection. The observation of snapshots (real time propagation of the seismic wave in the cross section) reveals that the seismic energy is scattered when hitting the rugged interface and the reflected wave is altered and forms a complex upgoing wavefield.

This observation confirms that the rough nature of a given interface is one of the reasons that alter the reflection event in spite of the presence of an abrupt velocity contrast.

Conclusion:

The geological structure of the Aigion fault could not be expressed by the surface seismic. The seismic reflection section was totally blurred in spite of the clear velocity contrasts revealed by the logging measurements. So, the VSP technique was investigated to identify the fault structure.

Using the 2D full wave modeling technique, the present case study focused on the reconstitution of the complex seismic wave propagation through the geological structure around the AIGION fault. This procedure allowed identifying the seismic wave behaviour in the fault vicinity (origin and travel path): as a result, some additional structural information has been derived. Mainly, we detected the presence of an additional fractured zone (FZ.2) that was accurately positioned. This fractured zone most probably expresses the presence of a secondary fault at shallow depth in the zone between the well AIG-10 and the main Aigion fault.

The presence of similar minor faults not involving the basement was confirmed by geologic observation of outcrops in the Aigion area. In addition, a rugged reflecting interface has been modelled in order to attempt explaining the absence of VSP reflection at the level of abrupt velocity contrasts observed in the well.

In addition, a rugged reflecting interface has been modelled in order to attempt explaining the absence of VSP reflection at the level of abrupt velocity contrasts observed in the well.